SINGLE MODE TUNABLE SHORT EXTERNAL CAVITY SEMICONDUCTOR DIODE LASERS

SINGLE MODE TUNABLE SHORT EXTERNAL CAVITY SEMICONDUCTOR DIODE LASERS

by

LEE JOHN BONNELL, B.Sc.

A Thesis

Submitted to the School of Graduate Studies

in Partial Fulfilment of the Requirements

for the Degree

Master of Engineering

McMaster University

January 1989

MASTER OF ENGINEERING McMASTER UNIVERSITY

(Engineering Physics) Hamilton,Ontario

TITLE: Single Mode Tunable Short External Cavity Semiconductor Diode Lasers

AUTHOR: Lee J. Bonnell, B.Sc. (University of Waterloo)

SUPERVISORS: Professor D.T. Cassidy and Professor J. Reid

NUMBER OF PAGES: ix, 83

ABSTRACT

This thesis describes the use of short external cavity (SXC) semiconductor diode lasers as single longitudinal mode (SM) tunable sources. A SXC forces a multimode diode laser to lase on a single longitudinal mode. Various laser types were investigated in SXC configurations using both planar and spherical external mirrors. The side mode suppression ratio (SMSR) and the SM tuning range were measured with respect to the positioning of the external cavity element. With a planar mirror as the SXC element, SMSR of –33 dB and SM tuning ranges of 1 nm (110% of a mode spacing) were obtained with inverted rib waveguide (IRW) lasers. For external cavity lengths of ~ 60 μm the total continuous SM tuning range summed over all modes was found to be 72 cm^{-1} or 12 nm. The use of a spherical mirror improved the results. A SXC laser consisting of a spherical mirror and an IRW laser had SMSR values of –37 dB and SM tuning ranges of 1.10 nm.

Power and voltage characteristics of SM SXC lasers were also examined. It was found possible to use the laser voltage and electronic feedback to control the external cavity length for optimum SM output. The external differential quantum efficiency (DQE) was found to be wavelength dependent and may be explained by the wavelength dependence of the scattering/absorption loss. One aspect of the characteristic trend of the DQE with respect to wavelength is that it offers the possibility of determining the lasing wavelength of the SM without the use of a monochromator.

AKNOWLEDGEMENTS

I would like to express my gratitude to my supervisor, Dr. Dan Cassidy for his guidance and assistance throughout the course of this work.

I would also like to thank my parents, John and Sara Bonnell, for their continuous support during my academic journey.

TABLE OF CONTENTS

LIST OF FIGURES

CHAPTER 1

INTRODUCTION

InGaAsP semiconductor diode lasers normally operate above threshold with several longitudinal modes containing a significant portion of the energy. This trait has been attributed to various mechanisms such as spatial and spectral hole burning, and to the role played by the spontaneous emission [1]. In many applications multimode spectral output is undesirable and one solution to this problem is the addition of a short external cavity to the laser diode. The short external cavity provides additional wavelength selectivity and hence, under proper alignment, forces a multilongitudinal mode laser to operate on a single longitudinal mode. Characteristics of the operation of short external cavities (SXC) semiconductor diode lasers have been extensively studied both experimentally [2–14] and theoretically [12–19]. The motivating factor for the studies is the use of SXC lasers as sources for optical communication systems since single mode operation is advantageous in dispersive optical fibers. Single longitudinal mode (SM) oscillation and a drastic reduction (relative to a solitary laser) of mode partitioning has been confirmed for high speed modulation of SXC lasers [5,7,9,12,14,20]. The temperature range over which the SXC laser maintains oscillation on the same longitudinal mode for changes in the heat sink temperature has been studied and used as a figure of merit of the quality of the SXC laser [11,20–22]. Techniques to maintain SM operation over large temperature ranges have been developed [11,20,21,25]. SM operation has been found for a temperature range of 25 $^{\circ}$ C with a planar [21] reflector. The noise induced by the SXC has been studied [4,6] as has

the side mode suppression ratio as a function of the external cavity length [8–12].

For these investigations the SXCs have been composed of planar reflectors [2,6,9,11,12,21], spherical reflectors [3,5,8,11–13], or waveguides [4,7,10,20] placed closer than ~1 mm to the laser facet. Despite the amount of work performed on SXC lasers there are still some relationships which are not known. For example, the accuracy to which the facet and SXC element must be aligned has not been investigated to any great degree. Renner and Carrol [3] found that the alignment restriction was not severe. Kuwahara et al. [6] noted that a $\pm 2^{\circ}$ tilt of the SXC element relative to the laser facet had negligible effect on their results. Lin et al. [9] obtained a 50–75 % yield for fabrication of SXC lasers by epoxying a mirror behind the laser. These results suggest a weak dependence of SXC operation on alignment though the dependence is not known. The amount that the optical frequency can be tuned is also not well known for SXC lasers. The SM tuning range is important in heterodyne and spectroscopic applications [24–26] where it is necessary to match the output wavelength to a given value.

This thesis reports on the use of SXC semiconductor diode lasers as single mode tunable sources. The underlying theory behind the operation of these devices is covered in Chapter 2. Section 2.1 outlines general diode laser theory and models the laser as a Fabry–Perot resonator enclosing an active medium [28,29]. Section 2.2 modifies the theory to account for the effects of a SXC by assigning a wavelength dependent reflectivity to the feedback facet [13]. The feedback is determined by calculating the coupling between the guided mode of the laser and the light reflected by the SXC element using a Guassian beam analysis [31]. An equation which describes the coupling efficiency as a function of the angular and positional orientation of the SXC element is derived in Sec. 2.3 . In Sec 2.4 the

theory is used to predict the side mode suppression ratio (SMSR) and single mode (SM) tuning range of SXC lasers as a function of the angular alignment of the external cavity. The SMSR is a ratio of the amplitude of the largest side mode to the main lasing mode. A laser is operating more SM as the SMSR decreases. The SM tuning range is defined as as the range over which the optical frequency can be tuned while maintaining the SMSR $\leq$ 1 % .

In the experimental phase of this thesis gain guided, inverted rib waveguide (IRW) and buried heterostructure (BH) 1.3 μm InGaAsP lasers and a 0.76 μm GaAs channeled–substrate planar–stripe (CSP) laser were examined in SXC configurations. Planar and spherical mirrors were used as the SXC element. The experimental technique is explained in Chapter 3. Chapter 4 presents the experimental results. Section 4.1 contains the SMSR and SM tuning range measurements which were measured with respect to the external cavity length and angular alignment of the SXC. These experiments reveal the alignment and positional tolerances of the SXC lasers as well as the dependence of the SMSR and SM tuning on the amount of optical feedback coupled back into the laser diode. The experimental values show qualitative agreement with the theoretical results of Sec. 2.3 . With the addition of a properly aligned SXC the SMSR could be improved from $\geq$ 50 % to $\leq$ 0.1 % and the optical frequency of a single mode could be tuned more than a mode spacing ($\geq$ 5.25 cm^{-1} or 0.89 nm).

In Sec. 4.2 several aspects of the laser power and voltage characteristics are examined to gain additional insight to the mechanisms involved in the operation of SXC lasers. The effect of a small modulation in the external cavity length is found to modulate the output power and the voltage across the laser diode. These power and voltage modulations can be used to lock the external cavity length for

optimum SM output. This technique has previously been demonstrated using the laser power [21] and in this thesis the technique was successfully applied using the voltage signal.

The external differential quantum efficiency (DQE) was measured by applying a small modulation to the laser current. Using a SM SXC laser the DQE could be measured with respect to wavelength simply by cycling through the cavity modes. The DQE is found to increase with wavelength for all laser types. This behavior is explained by a simple model which suggests that the scattering and absorption loss is wavelength dependent. A similar trend has been found utilizing other techniques [34,35]. One aspect of this characteristic wavelength signature is that the DQE provides a method of identifying the lasing wavelength without the use of a monochromator. The voltage modulation was also measured as a function of wavelength and shows an inverted relationship compared to the DQE.

In Chapter 5 a summary of the work is presented as well as recommendations for future work.

CHAPTER 2

BACKGROUND

2.0 Introduction

In this chapter the steady state operating characteristics of semiconductor diode lasers will be presented as well as the effects of introducing a short external cavity (SXC). Section 2.1 covers the theory that is used to generate a steady state laser model and Sec. 2.2 discusses the consequences of adding a SXC to a diode laser and the modifications required to the theory of Sec. 2.1 . The theory is used to model the spectral characteristics of SXC lasers and is presented in Sec. 2.3 . A summary then follows in Sec. 2.4 .

2.1 Semiconductor diode laser theory

A laser requires both optical gain and optical feedback to oscillate. In the case of semiconductor diode lasers optical feedback is provided by the reflectivity of the cleaved facets of the laser chip. The cleaves are along the {110} plane of the crystal and form a planar Fabry–Perot resonator. The reflectivity is ~ 0.32 for InGaAsP compositions. Forward biasing the diode laser creates an electron/hole inversion and thus produces optical gain. Lasing threshold occurs when the current is large enough such that the gain plus the spontaneous emission equals the loss. As the current is pushed past threshold the net gain (including spontaneous emission) briefly exceeds unity allowing the intensity to

build exponentially in the laser. The inversion quickly becomes depleted which clamps the net gain to unity thus maintaining the intensity in the cavity at a steady state level (ignoring quantum fluctuations). To analyze the steady state behavior of a diode laser above threshold, the laser is modeled as a Fabry–Perot cavity enclosing an active medium that contains gain and spontaneous emission. This is illustrated in Fig 2.1. The cavity has length l, electric field single pass gain g, spontaneous emission δ, and facet reflectances r_1 and r_2. The gain is assumed to be homogeneously broadened such that all electrons interact identically over the entire gain profile. The population in the lower level is taken to be zero, and rate equations are used to describe the gain of an infinitely thin section of the cavity. With this description of the laser, the electric field is then integrated over one round trip through the cavity. A simplified analysis is as follows. The steady state equation for the electric field at the z=0 facet, E_0^-, is found by following the field on one round trip through the cavity [27,28,29], and is given by

$$E_0^- = \frac{\delta^- + \delta^+ r_2\ g\ \exp(ikl)}{1 - r_1 r_2\ g^2 \exp(2ikl)} \tag{2.1}$$

where k is the wave vector defined as $2\pi/\lambda$ (λ – wavelength) and δ^+, δ^- are the spontaneous emission travelling in the positive and negative directions respectively. The intensity is found by multiplying (2.1) by its complex conjugate. The steady state value of the spontaneous emission is found by the time averaged quantities

$$\langle(\delta^-)^2\rangle = \langle(\delta^+)^2\rangle = \langle\delta^2\rangle \tag{2.2}$$

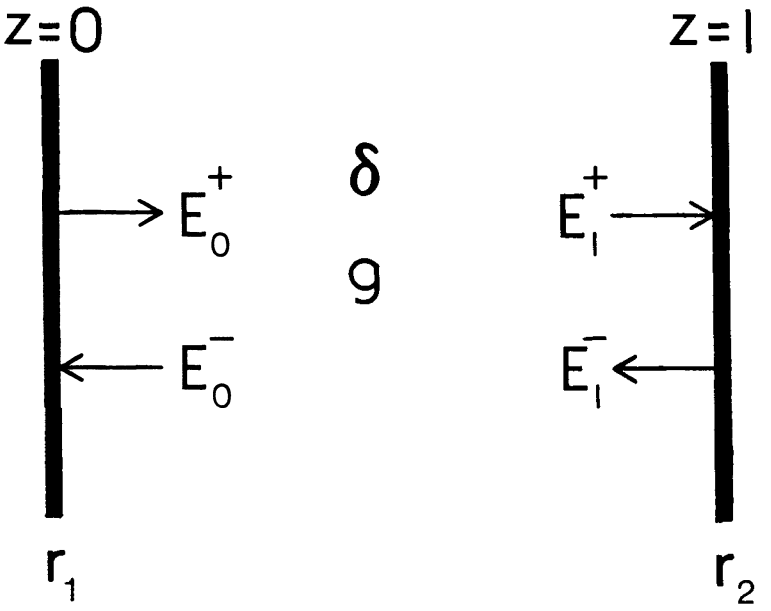

Figure 2–1: Pictorial representation of the semiconductor diode laser model. E_z^i are the electric fields for the forward (+) and backward (–) travelling waves at $z=0, l$. g is the single pass gain of the electric field and δ is the spontaneous emission. r_1 and r_2 are the facet reflectances.

and since δ^- and δ^+ are uncorrelated

$$<\delta^-\delta^+> = 0 \tag{2.3}$$

The equation for the intensity then reduces to

$$I_0^- = \frac{<\delta^2>(1+R_2G)}{(1-\sqrt{R_1R_2}G)^2 + 4\sqrt{R_1R_2}G\ \sin^2(2kl)} \tag{2.4}$$

where R_i $(=r_i^2)$ are the facet reflectivities and G $(=g^2)$is the single pass intensity gain. The resonator is a Fabry–Perot cavity and lasing occurs for modes which are separated in frequency by the free spectral range of the cavity given by c/2nl, where c is the speed of light and n is the refractive index. The power in a mode is determined by integrating the intensity over the free spectral range of the mode. Performing the integration one finds that

$$I_m^- = \frac{<\delta_m^2>\ (1+R_2G_m)}{(1-R_1R_2G_m^2)} \tag{2.5}$$

where m is the mode specifier, $<\delta_m^2>$ is the number of spontaneous photons emitted into the m^{th} mode and G_m is the single pass gain for the m^{th} mode. A proper formulation of $<\delta_m^2>$ and G_m requires a complete description of the active medium that includes pumping, lifetime, line shape, and saturation terms. A full analysis can be found in Ref. [28,29].

The spectral profile of the intensity gain has been found to

be approximately parabolic in shape with respect to frequency [29], and the mode nearest the gain peak will contain most of the lasers' output energy. The spontaneous emission decreases with wavelength but this dependence is minor in comparison to the effect of the spectral profile of the gain. An example of the mode spectrum for a gain guided laser is illustrated in Fig. 2.2 for various currents. Near threshold many modes contribute significantly to the total power, but as increases this number decreases due to the increased single pass gain. Another important result clearly shown in Fig. 2.2 is the tuning of both the gain profile and the mode wavelength to longer wavelengths. These characteristics are due to the increased heating of the active region. The temperature rise moves the bands closer together thus shifting the gain to longer wavelength. The refractive index of the active medium becomes larger as the temperature rises which shifts the cavity resonances to longer wavelength.

The use of solitary semiconductor diode lasers as single frequency sources thus poses some serious problems. The optical frequency of a laser mode may be tuned simply by altering the current through the laser. However, many modes may be lasing and a particular mode may contain a significant amount of energy only over a limited current range. The next section explains how the introduction of a SXC overcomes these limitations.

2.2 Effects of a short external cavity on laser operation

The introduction of a short external cavity results in optical feedback to the laser cavity. The geometry is shown in Fig. 2.3. The intensity in the laser cavity is determined by a similar analysis as performed in Sec. 2.1 . The intensity of

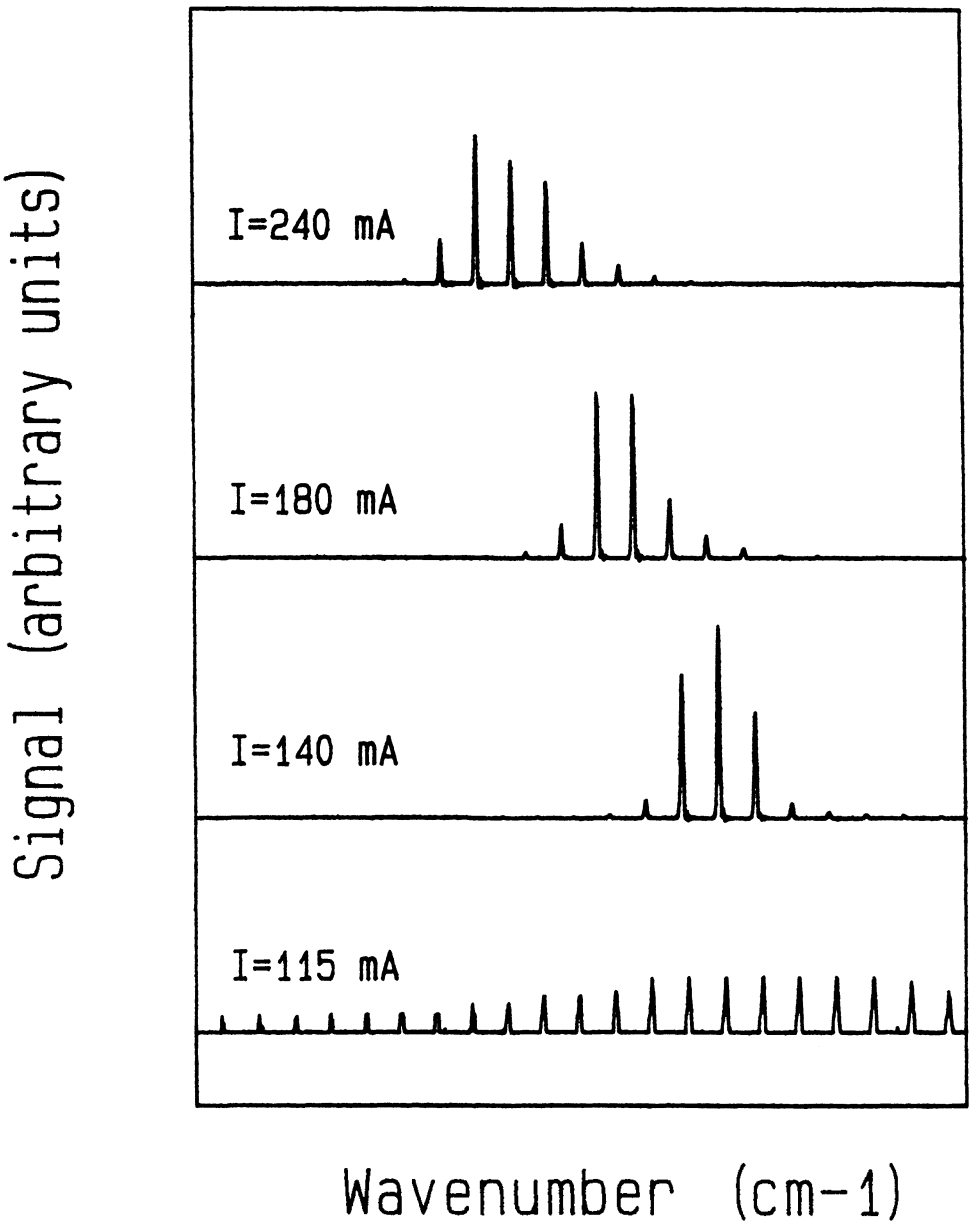

Figure 2–2: Example of the mode profile as a function of wavenumber for various injection currents. The zero level of each trace is offset for clarity. The data is from an IRW laser and the mode spacing is measured to be 5.25 cm^{-1}.

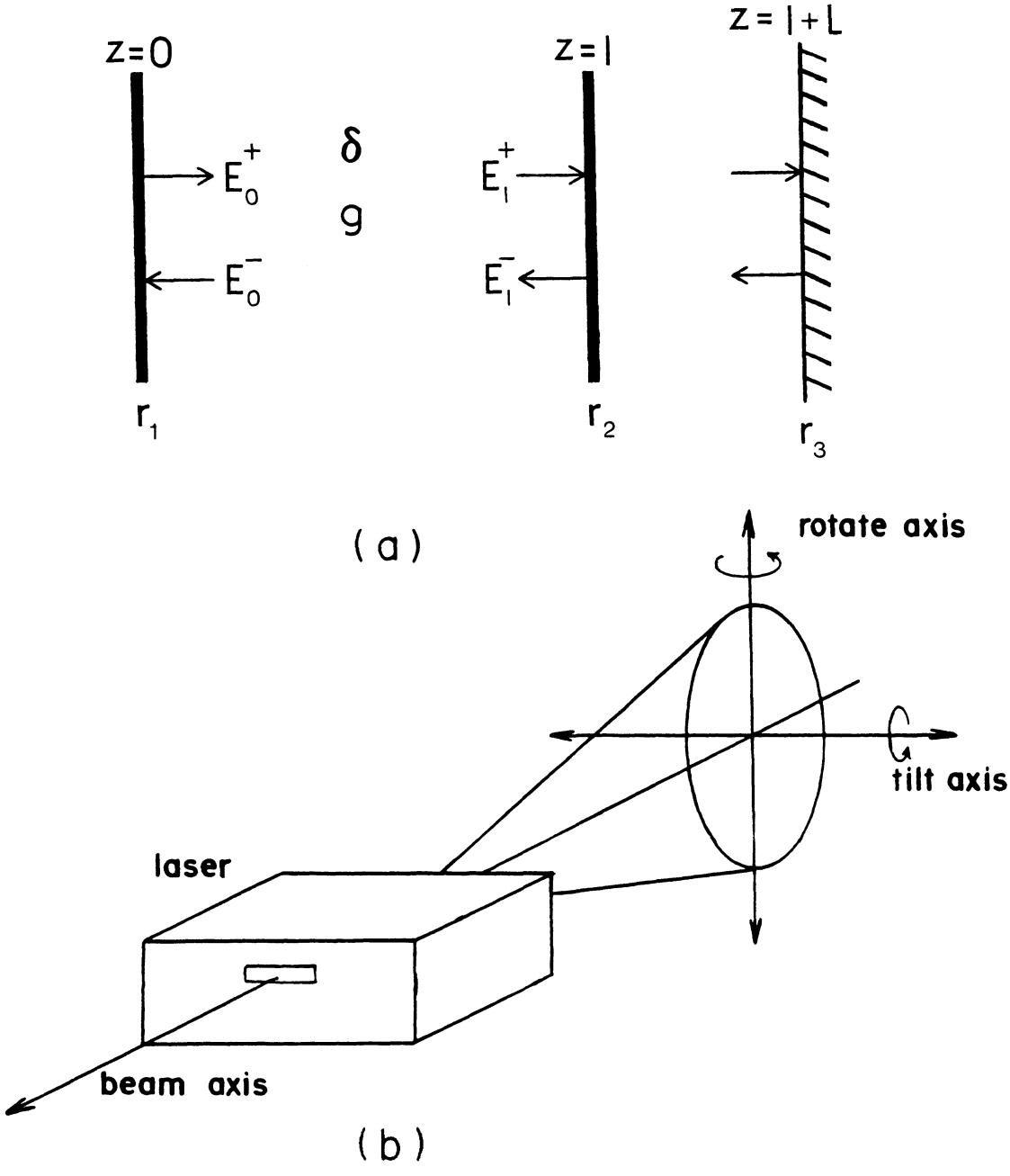

Figure 2–3: (a) Pictorial representation of an SXC laser. R_3 is the reflectivity of the external mirror, and L is the external cavity length.
(b) Off angle view of an SXC laser illustrates the tilt and rotate conventions. Rotation (|| to the plane of the active region) is about the vertical axis and tilt (⊥ to the plane of the active region) is about the horizontal axis

a mode is found to be

$$\bar{I_m} = \frac{<\delta^2>(1+R_{eff}G_m)}{(1-R_1R_{eff}G_m^2)} \tag{2.6}$$

R_{eff} is known as the effective reflectivity and an approximate value of R_{eff} is given by [13]

$$R_{eff} = R_2 + T^2R_3 + 2T\sqrt{R_2R_3}\cos(2kL) \tag{2.7}$$

where T is the intensity transmission of facet two and L is the length of the external cavity. R_{eff} has a large average term that is modulated by the wavelength dependent cosine term. Looking at Eq. (2.6) one can see that it has the same functional form as Eq. (2.5). Thus one can model the effect of the SXC by replacing R_2 by R_{eff} in the solitary laser, and the net result is a laser with one facet reflectivity which is wavelength dependent. Recognizing $(1-R_{eff})$ as the transmission loss, one can see that the effective reflectivity modulates the loss with respect to wavelength. The mode with the highest net gain has a lower threshold current and thus lases preferentially over other modes. The modulated loss term is apparent when observing the modes of a SXC laser near threshold and is illustrated in Fig. 2.4 . The top plot shows the modes of a solitary IRW laser near threshold. The lower plot is with a SXC when L = 160 μm. As the current increases beyond threshold the effect of the SXC is more dramatic as illustrated in Fig. 2.5 . Fig 2.5a shows the modes of a solitary IRW laser , with the modes being numbered 1 to 5 from long to short wavelength. With the addition of a SXC the

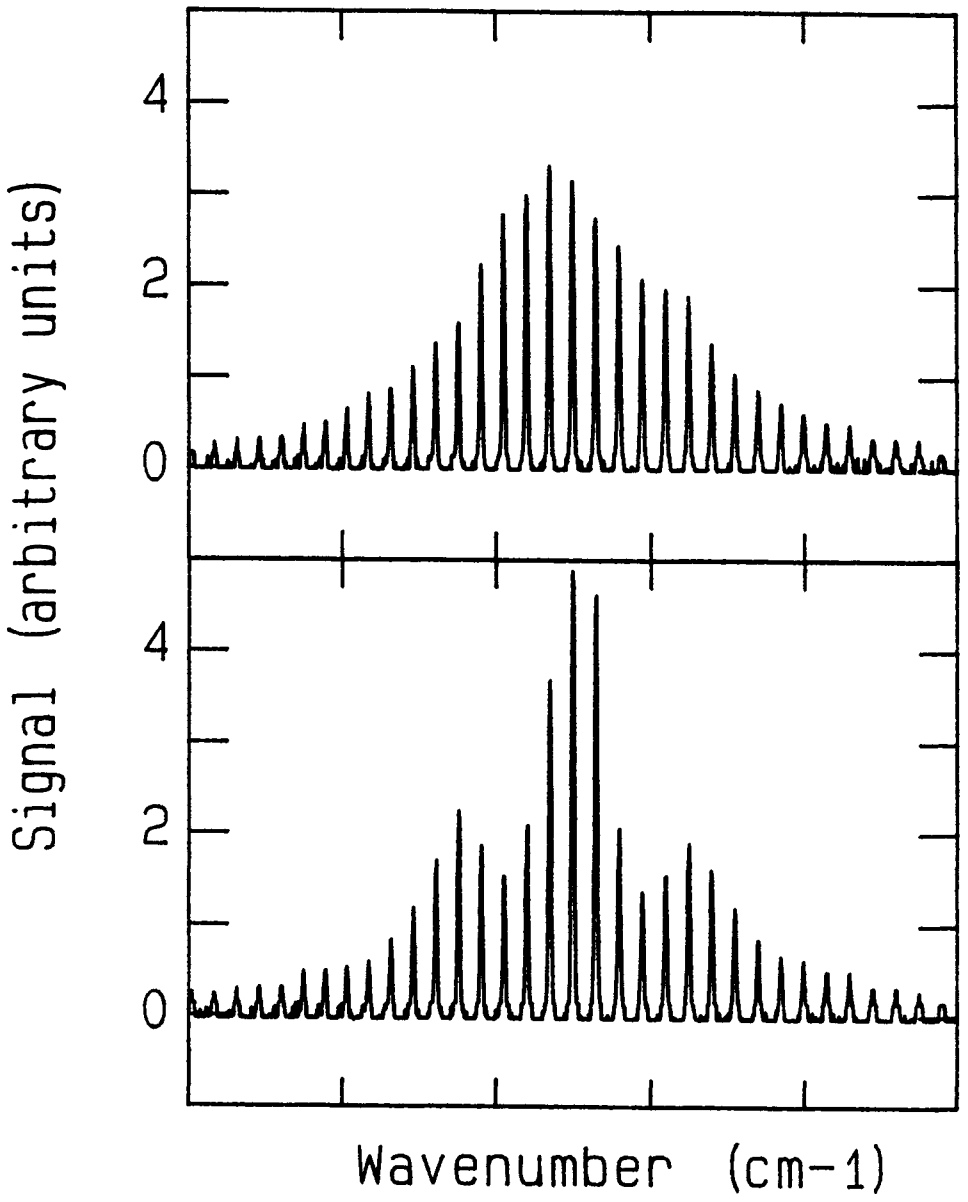

Figure 2–4: Mode profile of an BH laser near threshold (a) without feedback and (b) with feedback from a planar mirror at L=160 μm. This external cavity length corresponds to an external cavity mode spacing of 5 laser modes.

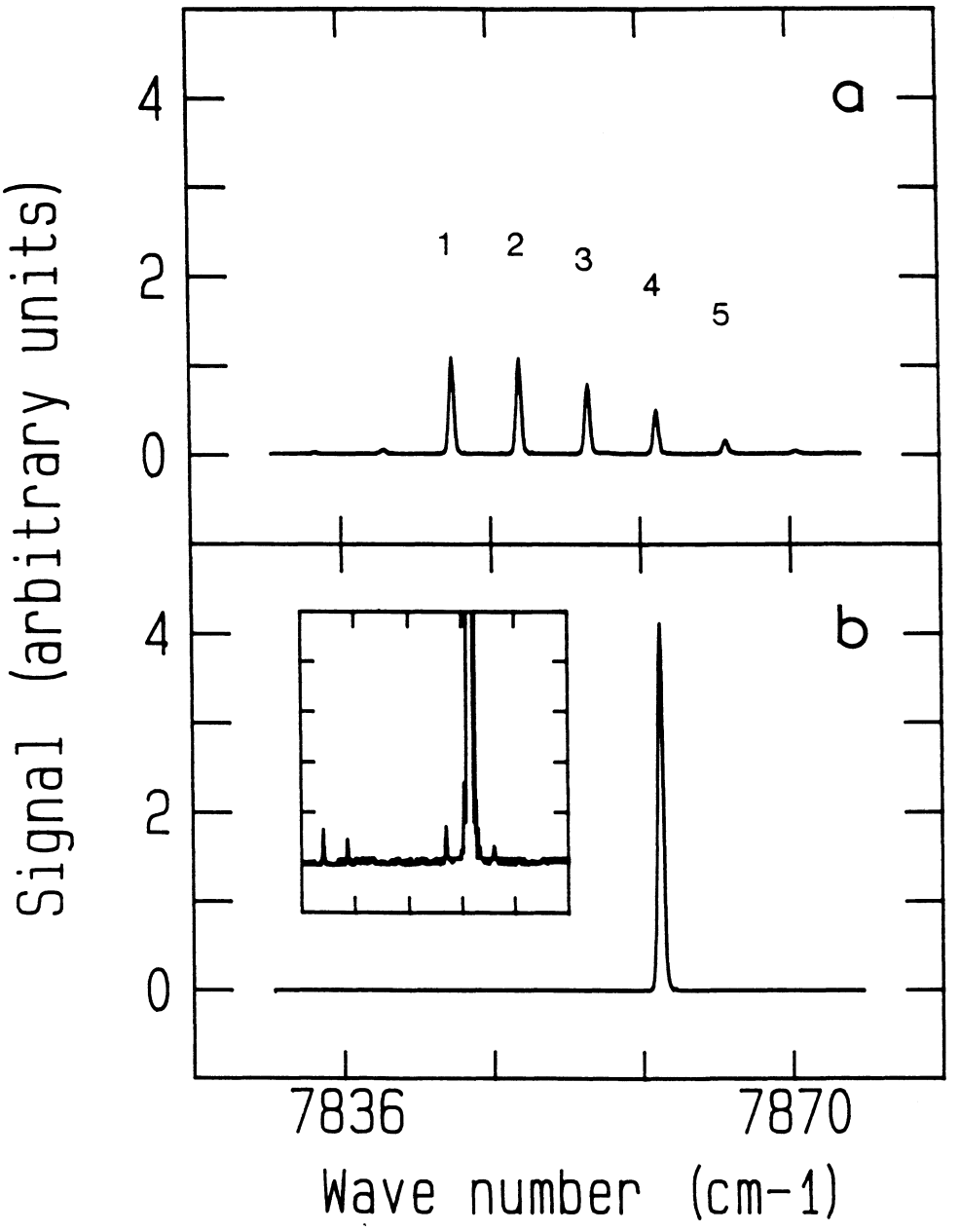

Figure 2–5: Mode profile of an IRW laser operating at $1.3 \times I_{th}$ (a) without feedback and (b) with feedback from a planar mirror at l=160 μm. The inset of (b) is expanded in the vertical direction 200 X and the SMSR is calculated to be 0.08 % (–31 db).

laser operates essentially single mode as illustrated in Fig. 2.5b where the external cavity is aligned to enhance mode 4. The inset window is expanded 200X in the vertical dimension. The ratio of the largest side mode to the main lasing mode is 0.08 % (–31 dB). By adjusting the length of the external cavity, single mode lasing could be obtained on any of the 5 numbered modes.

Thus resonant optical feedback can force a multimode laser to operate single mode. It is instructive to know the amount of feedback provided by the SXC. This knowledge allows one to determine the level of optical feedback over which a SXC can produce good SM output. The level of optical feedback is calculated by considering the coupling between the near field of the laser and the reflected far field at the laser facet [31]. The near field distribution can be inferred by measuring the far field at a known distance from the laser facet and then using beam propagation laws to find the field as a function of distance from the facet. The coupling is calculated by taking the overlap integral of the near field and reflected far field at the plane of the laser facet. The coupling efficiency is then the squared absolute value of the overlap integral. For the experimental geometry of the SXC as illustrated in Fig. 2.3b the equation for the coupling efficiency C, as a function of tilt angle θ_y, rotate angle θ_x, and external cavity length L, reduces to (see the appendix)

$$C = \tau_x \tau_y \cos^2(2\theta_x) \tag{2.8}$$

where

$$\tau_i = 2\frac{\omega_{oi}}{\omega_i}\exp[-\frac{k^2}{2}\omega_{oi}^2\sin^2 2\theta_i\,(1+\frac{L}{R_i}\cos 2\theta_i)]$$
$$\times \exp[-\frac{2L^2}{\omega_i^2}\sin^2 2\theta_i] \quad i=x,y \tag{2.9}$$

For these calculations the laser beam was assumed to be described by a Gaussian beam. ω_{oi} and ω_i are the beam waists of the near field and reflected far field respectively, and k is the wavenumber. The $\cos(2\theta_x)$ term is due to the polarization coupling of the reflected field and the emitted field and assumes lasing in the TE mode. There are three terms in (2.9) that can be interpreted by the following. The first term is a ratio of the beam waists and accounts for the coupling due to different beam sizes. The second term is an exponential which is a result of the angular coupling loss, and the third term is another exponential and gives the coupling loss due to the displacement of the reflected beam centroid.

Eq. (2.8) gives the coupling efficiency without considering reflection losses. The product of (2.8) times the surface reflectivity of the external mirror gives the overall reflectivity of the external mirror and is the term R_3 of Eq. (2.7). To apply the theory the far fields of the laser must be approximated by Gaussian profiles. The fit can be improved by using a linear superposition of Gaussians each having a unique amplitude, beam width, and angular offset (analogous to Fourier methods). Fig. 2.6a shows the measured far field intensities of an IRW laser and the fitted Gaussians. The fields were normalized with respect to the maximum intensity. The fitted far fields were approximated by a single Gaussian beam for the ($\|$) and ($\perp$) far fields. The parallel far field is parallel to the plane of the active region. Fig. 2.6b shows the calculated reflectivity of the external mirror with respect to angle for rotation ($\|$) and tilt ($\perp$). As illustrated in Fig. 6b, the

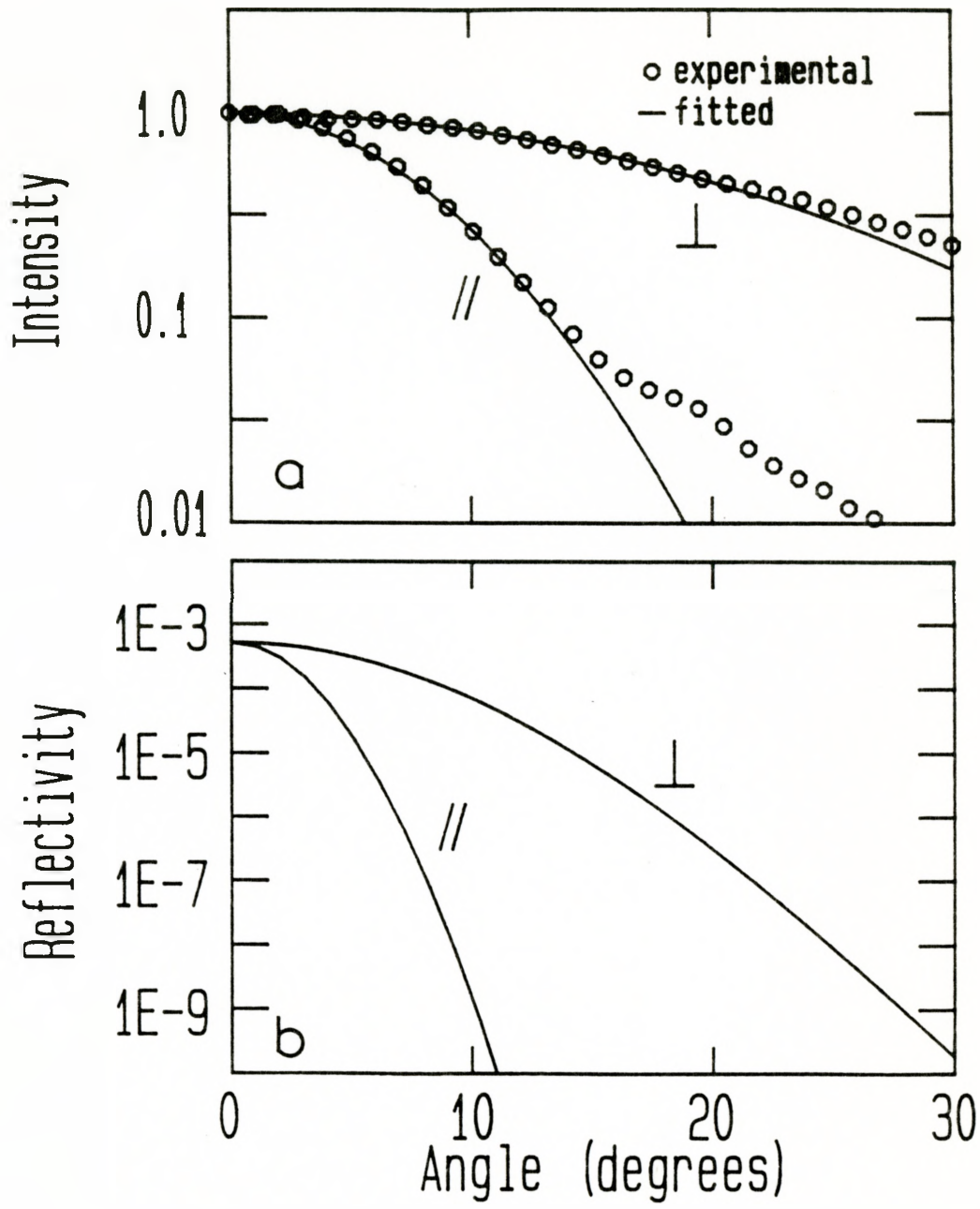

Figure 2–6: (a) Measured far field intensities for rotation (||) and tilt (⊥), and the fitted Gaussian profiles. The fit is composed of only one Gaussian for each far field.

(b) The calculated reflectivity as a function of rotation and tilt resulting from an external cavity at L=160μm and using the fitted far fields from (a).

reflectivity is estimated to be 5.2×10^{-4} at normal alignment and as the mirror is rotated the reflectivity decreases exponentially.

The values of R_3 can now be applied to the SXC laser model to predict the SMSR and SM tuning range.

2.4 Modeling results

A SXC laser was modeled to determine the SMSR and SM tuning range. The aim of this exercise is to examine the results on a qualitative level only, and thus a simple analysis is presented without detailed fitting to match experimental parameters.

The model parameters are outlined in Ref. [29] and the only modification necessary is the replacement of R_2 with R_{eff}. Only the mode at the center of the gain profile and one adjacent mode will be studied. R_3 is determined using the coupling equation and then inserted into the equation for R_{eff}. The external cavity length is set to match experiment and $R_1=R_2= 0.32$. The pumping level was maintained at a constant value which was determined to approximate experiment. For the SMSR the only variable altered was the value of R_3. To model the SM tuning range the spectral position of the gain peak was linearly tuned with pumping to approximate the experimental gain shift.

The model simulates the laser and outputs the energy in each mode as a function of pumping. Figure 2.7 is an example of the mode spectrum just above threshold with and without optical feedback. Figure 2.7a presents the idealized mode spectrum of a solitary laser and shows that many modes lase near threshold. The mode at the center of the gain profile has the largest intensity. With optical

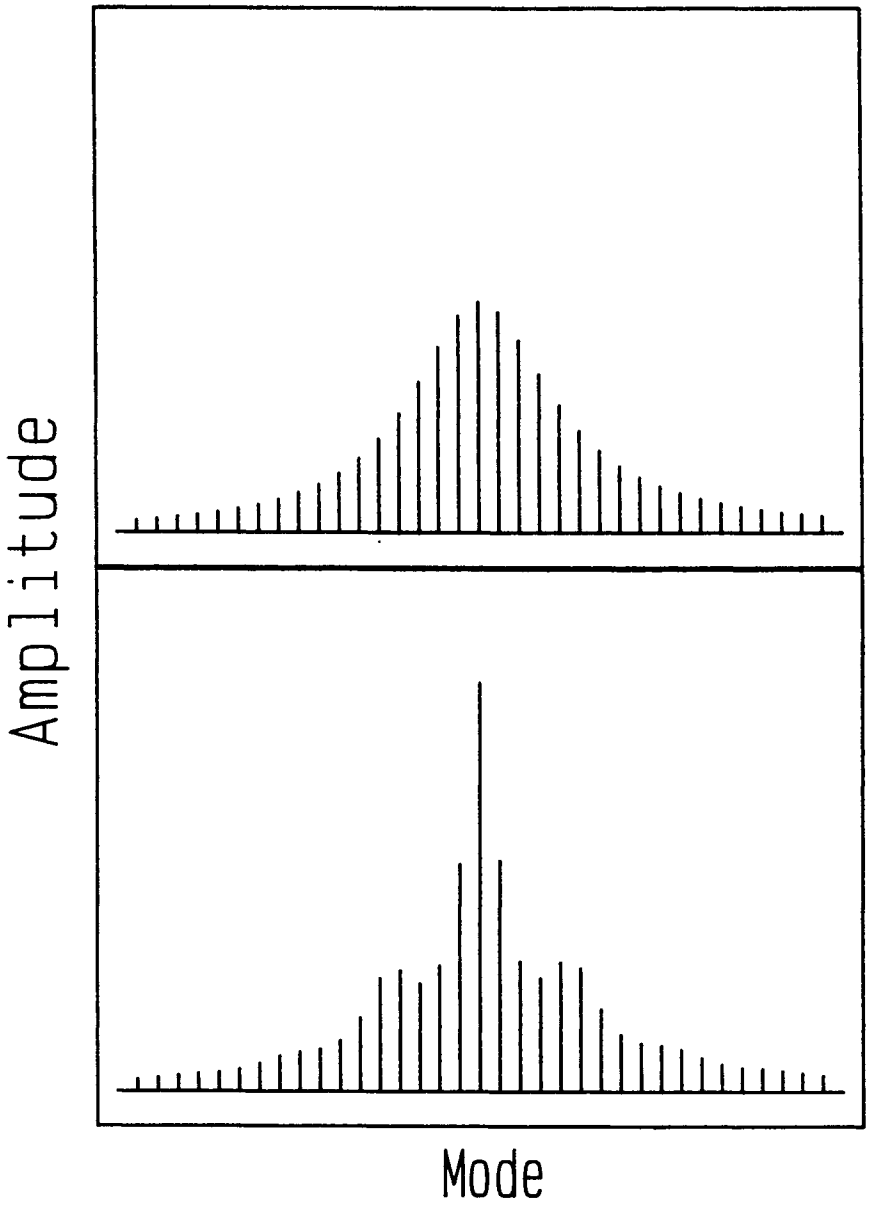

Figure 2–7: Theoretical mode profile of a diode laser near threshold for (a) a solitary laser and for (b) a laser with feedback from an external cavity of L=160 μm.

feedback of 1×10^{-4}, an external cavity set to L=160μm, and the external cavity set to enhance the central mode the resultant mode profile is illustrated in Fig. 2.7b . The modulation of the loss due to $(1-R_{eff})$ is apparent. Comparing Fig. 2.7 to Fig. 2.4 , the results agree qualitatively.

To model the SMSR and SM tuning range of a SXC laser certain parameters were chosen to match an IRW laser. The pumping level was set to be approximately $1.3\times I_{th}$. The external cavity length was set to be equivalent to 160 μm ($\sim$ 5 mode spacings). The gain, spontaneous emission and the remaining variables were taken from Ref.[29]. The theoretical results for the SMSR and SM tuning as a function of mirror rotation are presented in Fig. 2.8 . The SMSR is shown in Fig. 2.8a. At normal alignment the SMSR is at a minimum value of 0.003% (–45 dB) and as the mirror is rotated the SMSR increases until at $\theta = \pm 8^{\circ}$ the SMSR is 0.8 (–21 dB) for the mode 1 .

The SM tuning range is illustrated in Fig. 2.8b. At normal alignment the SM tuning range is 5 cm^{-1} (0.85 nm) for mode 1 at normal alignment, and decreases as the mirror is rotated. At $\theta = \pm 6^{\circ}$ the SM tuning range has reduced to $\sim$ 2.7 cm^{-1} (0.45 nm).

The modeling results offer a qualitative survey of how an SXC diode laser will operate with respect to the rotational alignment of the external mirror. To model the SXC laser precisely the parameters of the solitary laser must be matched to experiment.

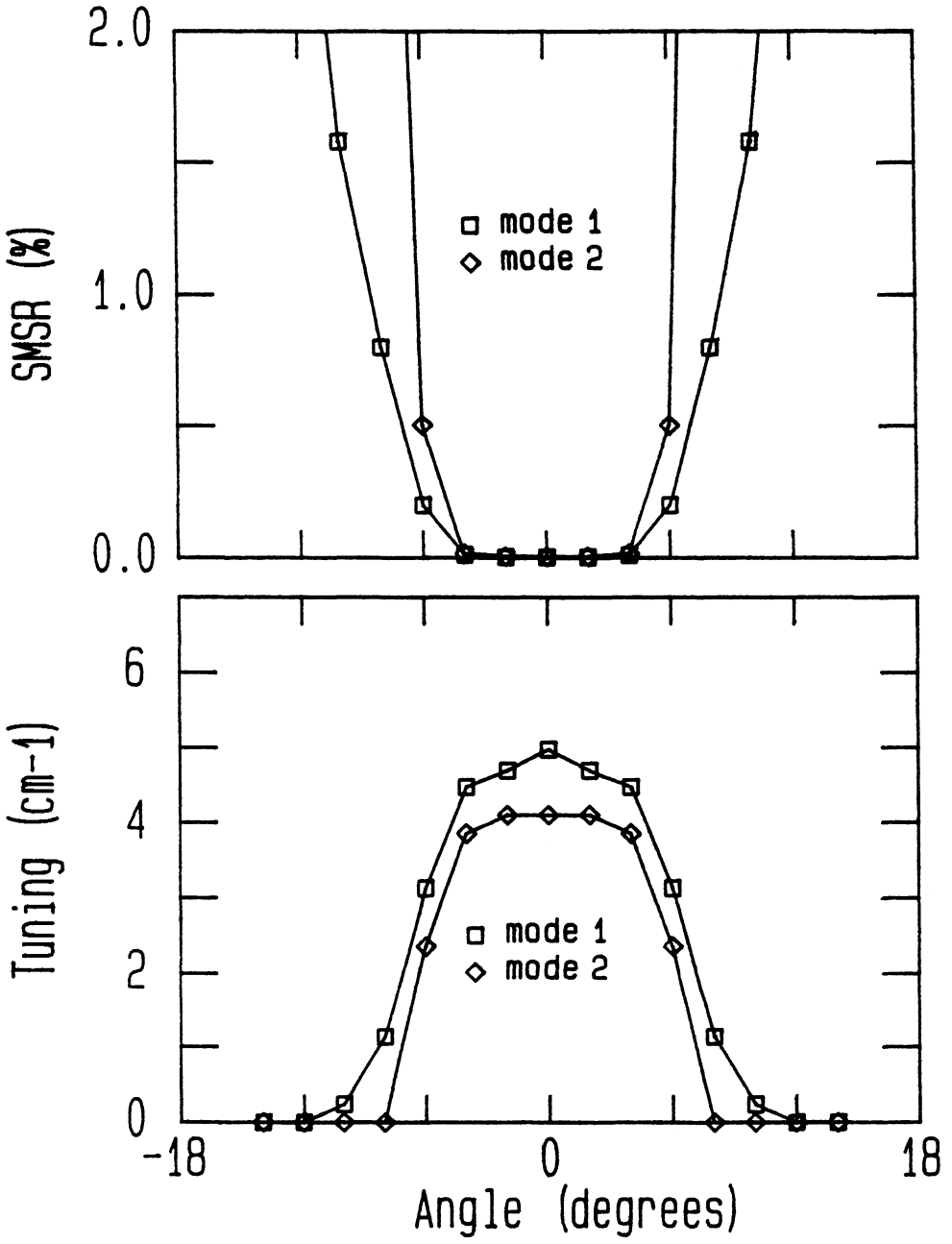

Figure 2–8: Plots of the theoretical (a) SMSR in % and (b) SM tuning range in cm^{-1} as a function of rotation angle of the external mirror. L was set to 160 μm.

2.5 Summary

In this chapter the general theory of semiconductor diode lasers was presented in Sec. 2.2 . The theory was modified in Sec. 2.3 to account for the effects of a short external cavity. The result was the replacement of the external cavity formed by the output facet and external mirror by a single facet having an effective reflectivity, R_{eff} , that was wavelength dependent. An expression for the amount of optical feedback was derived by considering the coupling between the beam at the laser facet and the reflected beam. The theory was used to develop a model of the SXC laser system. The side mode suppression ratio (SMSR) and single longitudinal mode (SM) tuning range (SMSR $\leq$ 1%) were modeled and the results were presented in Sec. 2.4 . At optimum alignment of the external cavity element (i.e. maximum feedback) the model predicts SMSR of $\leq$ 40 dB and SM tuning ranges of up to 5 cm^{-1}.

CHAPTER 3

EXPERIMENTAL TECHNIQUE

3.1 Introduction

In this chapter the experimental procedures will be outlined. The experimental technique is presented in Sec. 3.2 . The optical tuning of the laser modes, and the experimental far fields used to calculate the amount of optical feedback, are presented in Sec. 3.3 . A summary follows in Sec. 3.4 .

3.2 Experimental technique

Figure 3.1 is a schematic diagram of the experimental setup. The external reflector was mounted on a calibrated tilt and rotate stage that was attached to an XYZ translator. This allowed angular and positional alignment of the external cavity. The stage supporting the laser package was mounted on a piezo–electric translator (PZT) that allowed fine adjustment to the external cavity length. A high voltage supply with AC/DC inputs controlled the PZT. The rotate angle was about the vertical axis and the tilt angle was about the horizontal axis as previously illustrated in Chap. 2, Fig. 2.3 . Parallel alignment of the external cavity element and the laser facet is termed normal alignment since the beam axis is normal to the plane of the mirror. Experimentally it was necessary to establish the position of normal alignment. Two simple methods were found. One was by measuring the external differential quantum efficiency (DQE) of the laser as

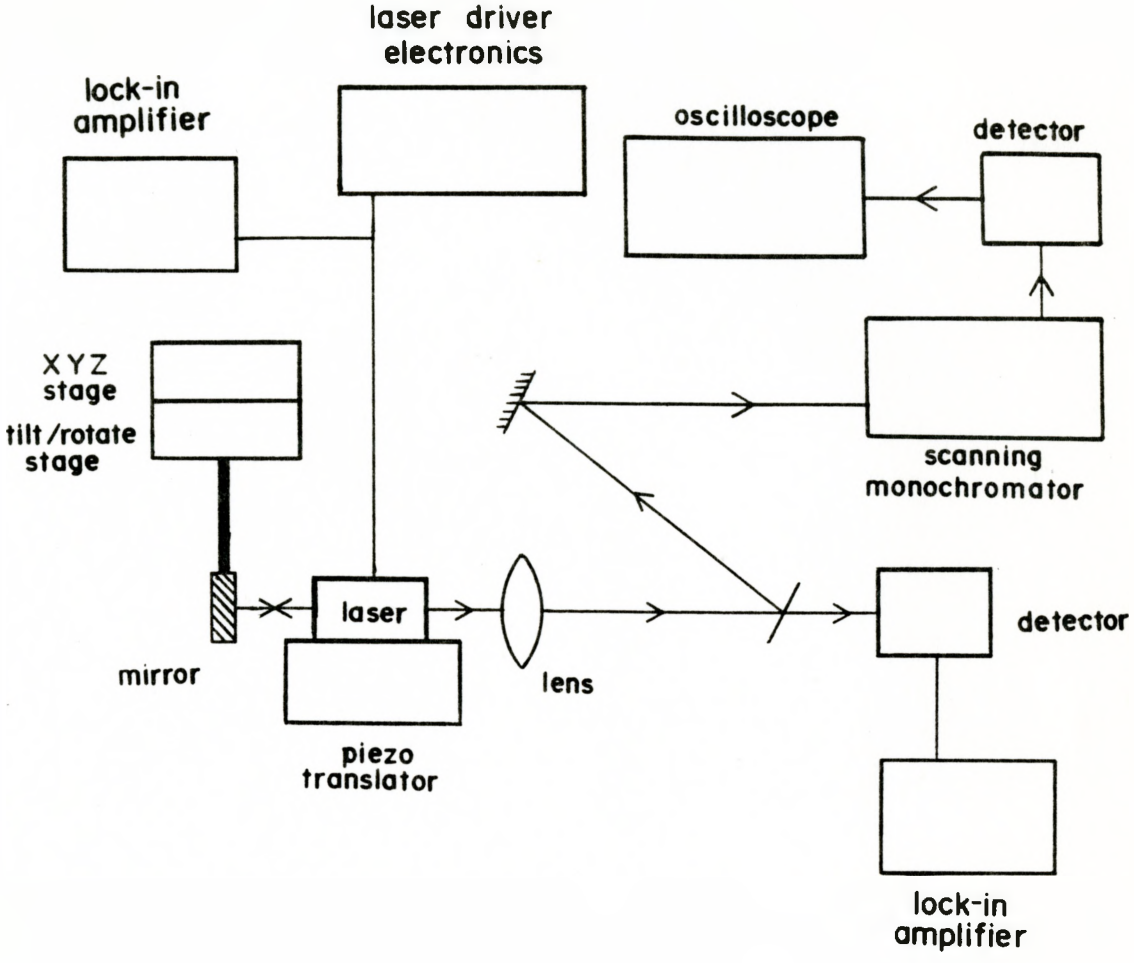

Figure 3–1: Schematic diagram of the experimental apparatus.

a function of tilt and rotate angles. The DQE is a maximum when the external mirror is aligned normal to the beam axis (see Chapter 4.2). A second method of aligning the mirror was by observing the interference pattern created by the output beam and reflected beam. The output beam and the reflected beam have different radii of curvature and form a ring interference pattern which is best observed with an IR viewer. The external mirror is aligned when the center spot of the interference pattern coincides with the center of the output beam. Planar and spherical mirrors were used. The planar mirror could be lowered until it rested on a piece of aluminum shim stock that was placed between the laser package floor and the mirror bottom. This reduced mechanical vibrations in the support arm of the external mirror which were found to limit the stability of the single mode SXC laser. The spherical mirror could not be similarly supported due to the alignment requirements of the optic axis. The only position that supported the spherical mirror was when the external cavity length was reduced until the mirror was resting against the face of the laser. This is potentially dangerous to the facet and thus was only attempted for one laser.

The planar mirror was a standard Au coated, polished diamond heat sink (400×400×250 μm). The surface roughness is given as 400 Å which is much less than the wavelengths considered (8000–13000 Å). Spherical mirrors were constructed from a planar aluminum plate. The surface was sequentially polished with increasingly finer polishing paste. The final paste was a 0.3 μm silica grit. The surface was found to have good mirror–like qualities. A spherical ball bearing of 400 μm (supplied by Industrial Tectonics, Dexter, Michigan USA) diameter was then pressed into the surface to form a spherical mirror. The mirrors were coated with a protective layer of polyimide and then cut from the plate with a diamond

saw. A surface analysis was performed on the polished plate prior to impression. A peak–peak surface variation of 500 Å was found over large ($\geq$ 100 μm) sections.

Measurements were performed on two gain guided, two IRW, and two BH 1.3 μm lasers and one 0.76 μm CSP GaAs laser. The spectral output was monitored using a scanning monochromator and an oscilloscope. A 1/2 meter monochromator was used and its resolution curtailed any studies of linewidth effects. The side mode suppression ratio (SMSR) is defined as the ratio of the largest side mode to the main lasing mode. The single mode tuning range is defined to be the range over which a mode would maintain a SMSR $\leq$ 1% . The monochromator broadened the linewidth of the modes equally, and therefore the SMSR is a ratio of the mode energies. The SM tuning range was measured by monitoring the modes while changing the injection current. The external cavity length was manually optimized for SM output for the SMSR and SM tuning range measurements.

The power and voltage of SXC lasers were examined. Modulations of the power and voltage were monitored with lock–in amplifiers. To minimize both transmission fringes and optical feedback caused by the output collecting lens, a 10X optical attenuator was placed between the laser and lens. The injection current was modulated by the laser controller. The external cavity length was modulated using the AC inputs of the high voltage piezo–electric controller.

3.3 Tuning calibrations and far fields

The optical tuning of the modes were calibrated with respect to the injection current. The mode spectrum was recorded at various currents and the

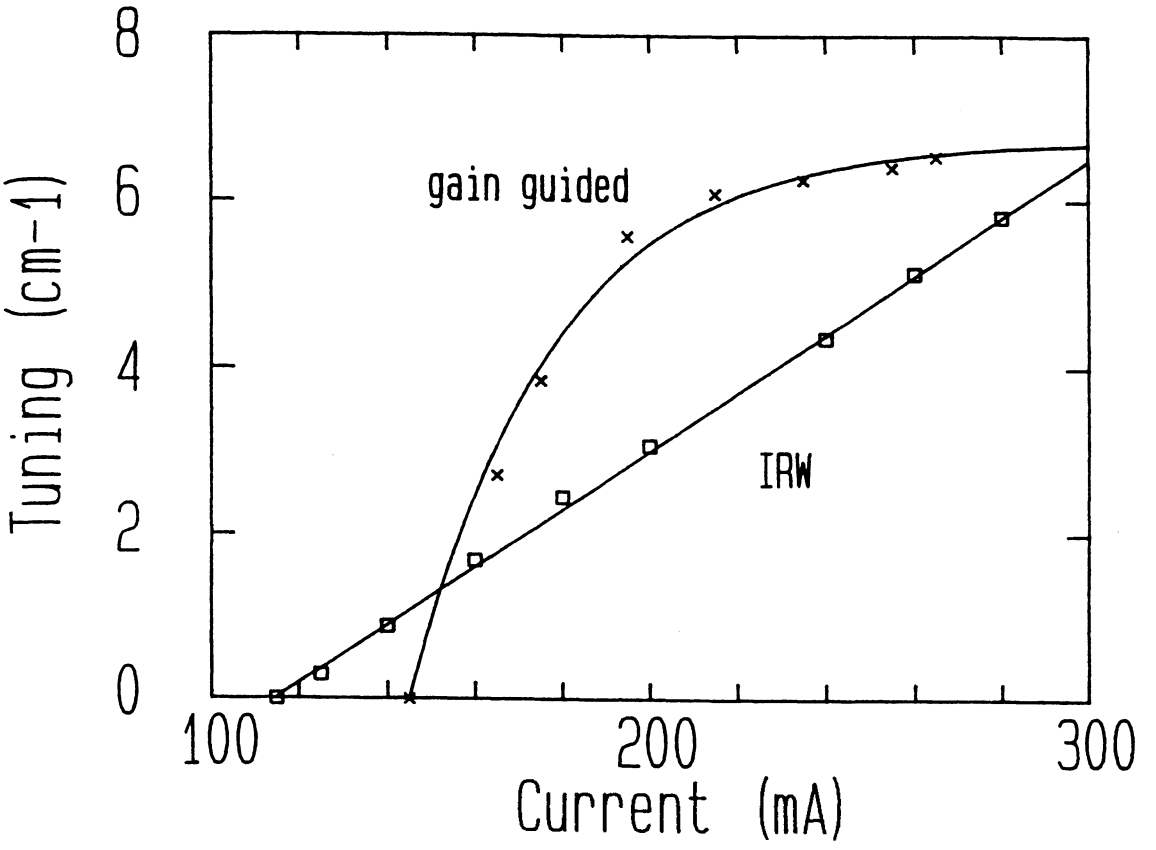

Figure 3–2: Optical tuning of the mode wavelength as a function of injection current for gain guided and IRW lasers.

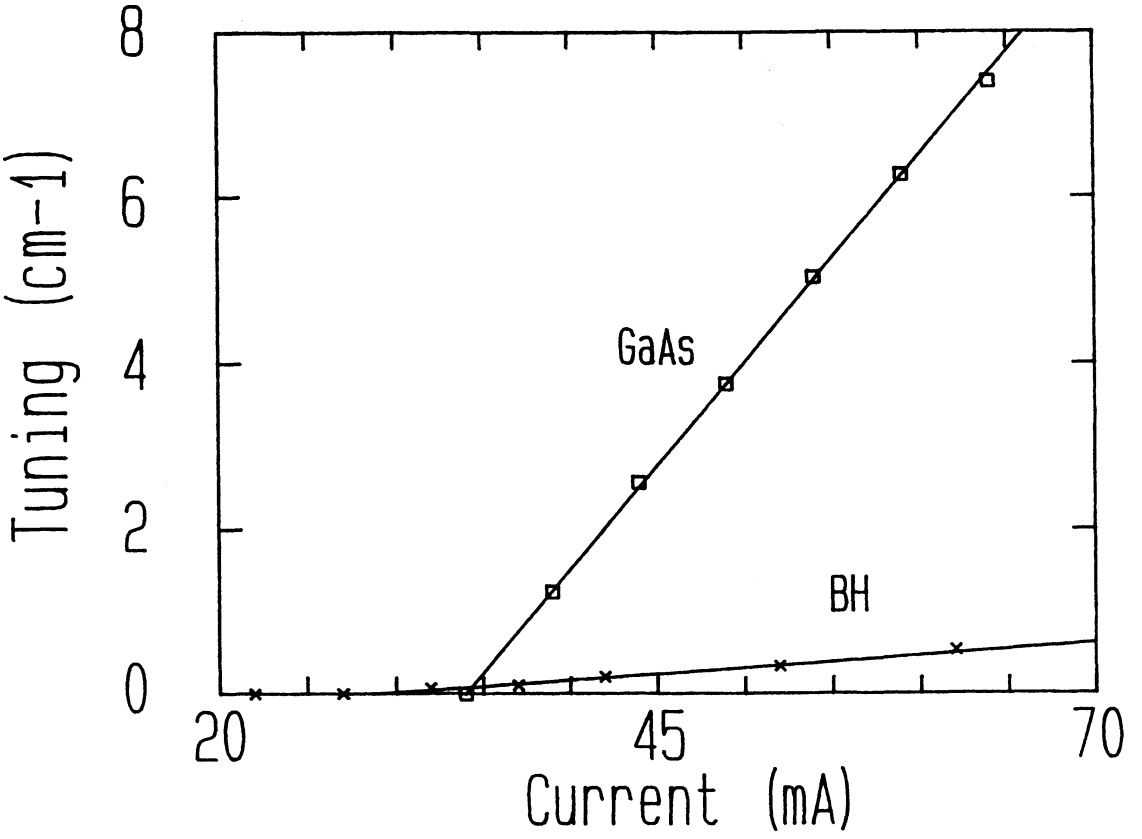

Figure 3–3: Optical tuning of the mode wavelength as a function of injection current for BH and GaAs lasers.

frequency tuning was determined using the measured mode spacing as a reference. The tuning calibrations for the lasers are shown in Fig. 3.2 and 3.3 . Fig. 3.2 presents the tuning results for a gain guided laser and an IRW laser. The tuning of a gain guided laser with respect to the injection current saturates at high injection currents. The IRW laser has a lower threshold current and it tunes linearly with current. Figure 3.3 shows the results for the 1.3 μm BH laser and the CSP GaAs laser. Note the much lower threshold currents provided by the BH and CSP structure. Both lasers exhibit a linear tuning trend with respect to current. Interestingly, the BH laser shows a very minimal tuning trend. The reason for this discrepancy is not clear and it may be that the internal resistance of the BH laser is relatively small thus creating only minimal joule heating. Another factor may be that the non–radiative recombination is very low for this device as compared to the other laser types. The tuning trends were fitted with curves to give the tuning calibration.

To determine the amount of optical feedback the far fields of the lasers had to be known. The far fields were measured with a multimode optical fiber affixed to the external mirror mount. The fiber was translated perpendicular to the beam axis such that a measurement was made every degree in the tilt/rotate transformation. The far fields were checked with a slit and detector to make sure that the fiber response was uniform with angle. Both measuring systems were found to provide similar results. The optical feedback is calculated (as described in Chapter 2) as a function of rotation angle only. The measured far fields and the calculated reflectivity of the external cavity are illustrated in Fig. 3.4 to 3.6 for an IRW, gain guided, and a BH (1.3 μm) laser. The IRW and gain guided lasers were fitted with a single Gaussian for the ($\perp$) far fields, and a summation of two

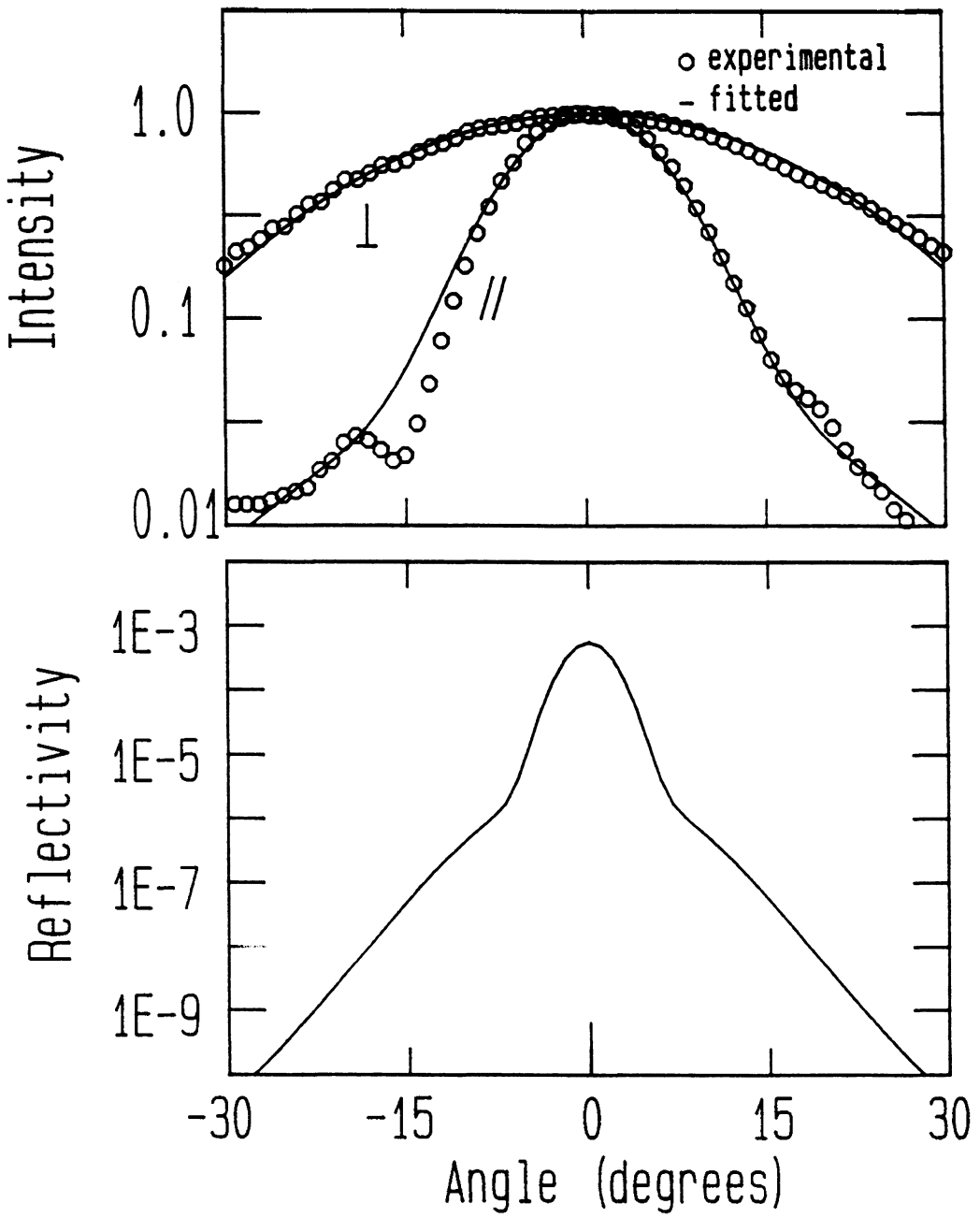

Figure 3–4: Plots of the far field intensity distribution and the theoretical reflectivity of the external mirror for an IRW laser. The far fields in (a) show the experimental values of the parallel (||) and perpendicular (⊥) fields and the fitted Gaussian fields as a function of angle. The reflectivity in (b) is plotted as a function of rotation.

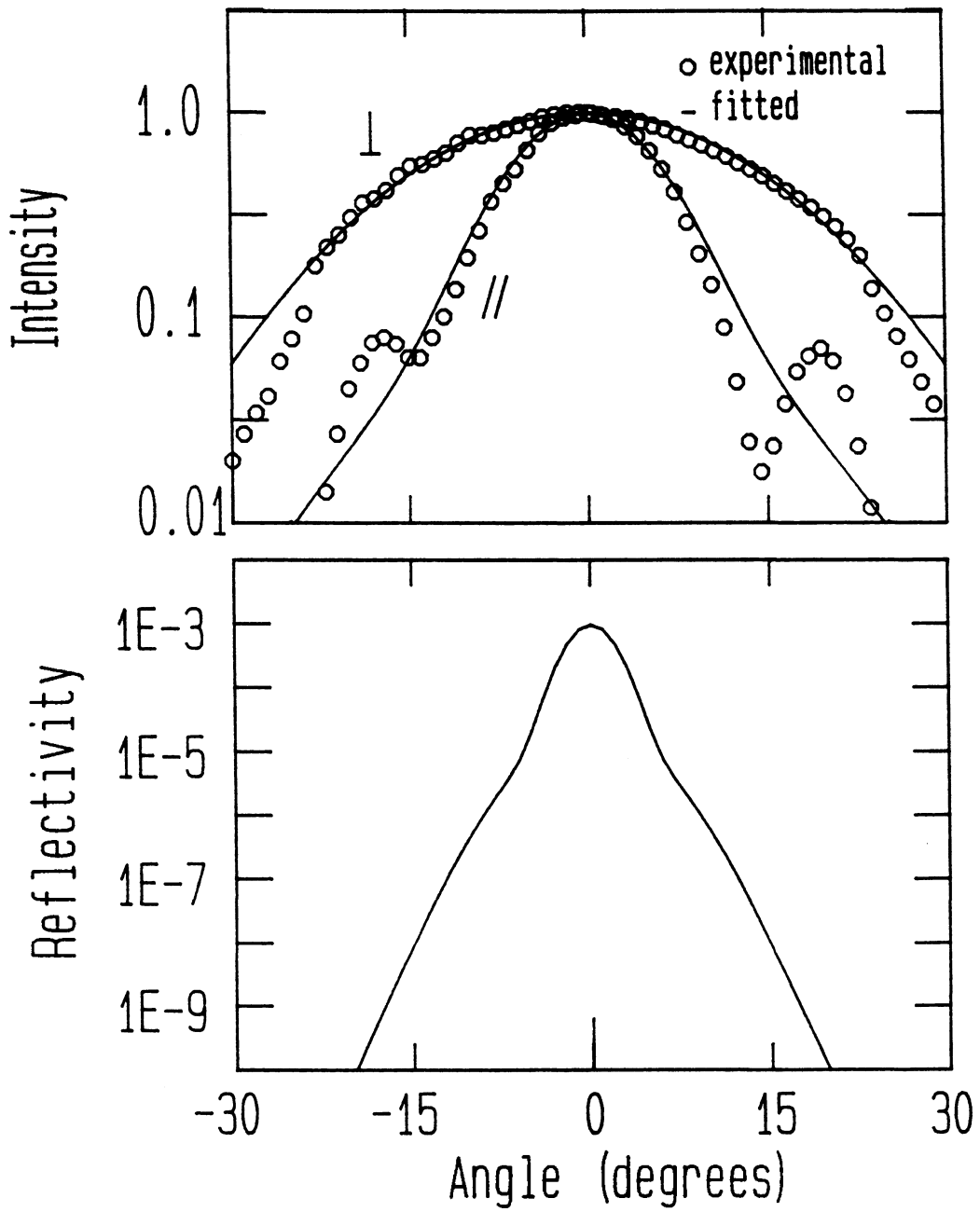

Figure 3–5: The same measurement as Fig. 3–4 for a gain guided laser.

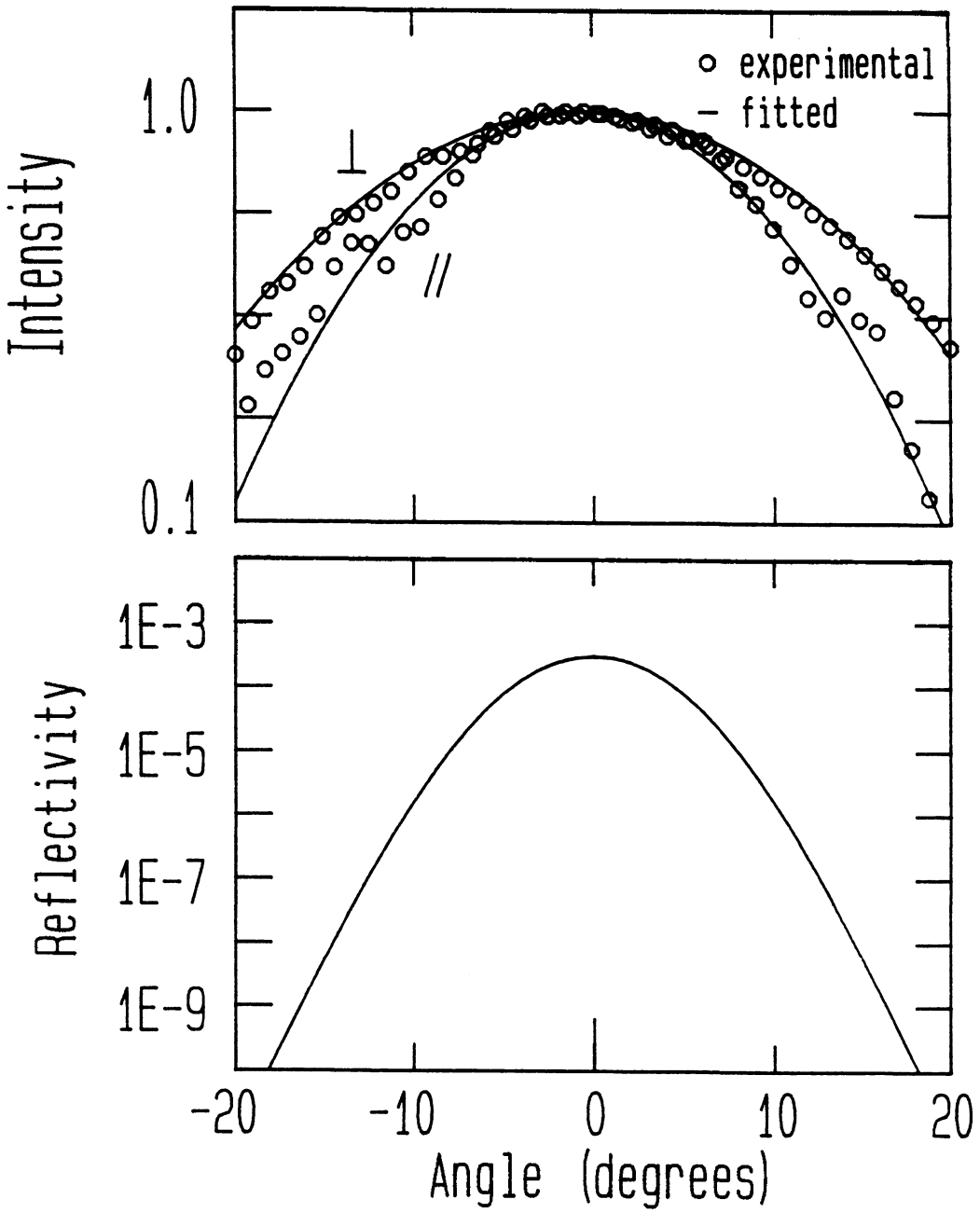

Figure 3–6: The same measurement as Fig. 3–4 for a BH laser.

Gaussians for the (||) far fields. The 1/e points for the far fields of the IRW laser shown in Fig. 3.4 are as follows. The ($\perp$) field consisted of one gaussian with a 1/e angle of 22°. The (||) field was composed of two gaussians with 1/e angles at 8° and 22°, and magnitudes of 95 % and 5 % respectively. A good fit for the BH laser required only a single Gaussian for each far field. The 1/e angles were measured to be 13.5° for the (||) field and 18° for the ($\perp$) field. The far fields for the GaAs laser were not measured but were observed to be similar to the IRW and gain guided lasers.

3.4 Summary

In this chapter the experimental technique was outlined. The tuning was calibrated by measuring the mode profile for varying injection currents. The amount of optical feedback was determined by fitting the measured far fields with a linear superposition of Gaussian beams.

CHAPTER 4

Experimental results

4.1 Introduction

The side mode suppression ratio (SMSR) and single longitudinal mode (SM) tuning range were investigated for gain guided, inverted rib waveguide (IRW) and buried heterostructure (BH) 1.3 μm InGaAsP diode lasers, and for a 0.76 μm channeled–substrate planar–stripe (CSP) GaAs laser. The SMSR and SM tuning range were measured with respect to **(a)** external cavity length and **(b)** rotational alignment of the external cavity element. These measurements are presented in Sec. 4.2 . Several aspects of the laser power and the voltage across the laser diode were also examined as a function of the external cavity orientation. The differential quantum efficiency (DQE) of the laser was measured as well as the power and voltage effects resulting from a modulation of the external cavity length. The power and voltage measurements are presented in Sec. 4.3 . A summary then follows inSec. 4.4.

4.2 Side mode suppression and single mode tuning range

The SMSR and SM tuning range of SXC semiconductor diode lasers were measured to judge their performance as single longitudinal mode tunable sources. Previous studies have found SMSR values of – (23–27) dB for BH InGaAsP lasers with planar reflectors [9,10,19]. Anti–reflection coating the feedback facet couples

more reflected light back to the laser and this has been found to reduce the SMSR to – (35–40) dB [19]. Spherical mirrors have also been utilized to increase the level of feedback and have produced SMSR levels of – (28–31) dB [8,12].

The non–continuous [3,8] and continuous [21] tuning ranges of SXC lasers have also been studied. Non–continuous tuning ranges of 10 nm have been found with spherical SXC lasers [8]. Planar mirror SXC lasers have provided continuous tuning ranges of 2 nm using very short laser cavities (135 μm) which spread out the mode spectrum with respect to wavelength (2 nm = 1 mode spacing) [21].

The work reported on in this chapter extends the results found in previous work. For example, the SMSR and SM tuning range results are investigated for more than one mode and the results are related to the amount of optical feedback reflected to the external cavity. The alignment tolerances are examined to determine the requirements for optimum performance of SM tunable SXC lasers. Power and voltage characteristics of SXC lasers were also examined to improve the utility of SXC lasers.

4.2.1 Inverted rib waveguide (IRW) lasers

The SMSR and SM tuning range measurements for an IRW laser with a planar SXC element are presented in Figures 4.1 to 4.3 . Fig. 4.1 shows the SMSR and SM tuning range with respect to the rotation angle of the external mirror. The measurements were performed for 5 adjacent modes centered in the gain profile. The SMSR in Fig. 4.1a is a minimum of 0.05 % (–33 dB) for mode 2 at a rotation of + 2°. At this rotation the average SMSR for the five modes was 0.07 % (–32 dB).

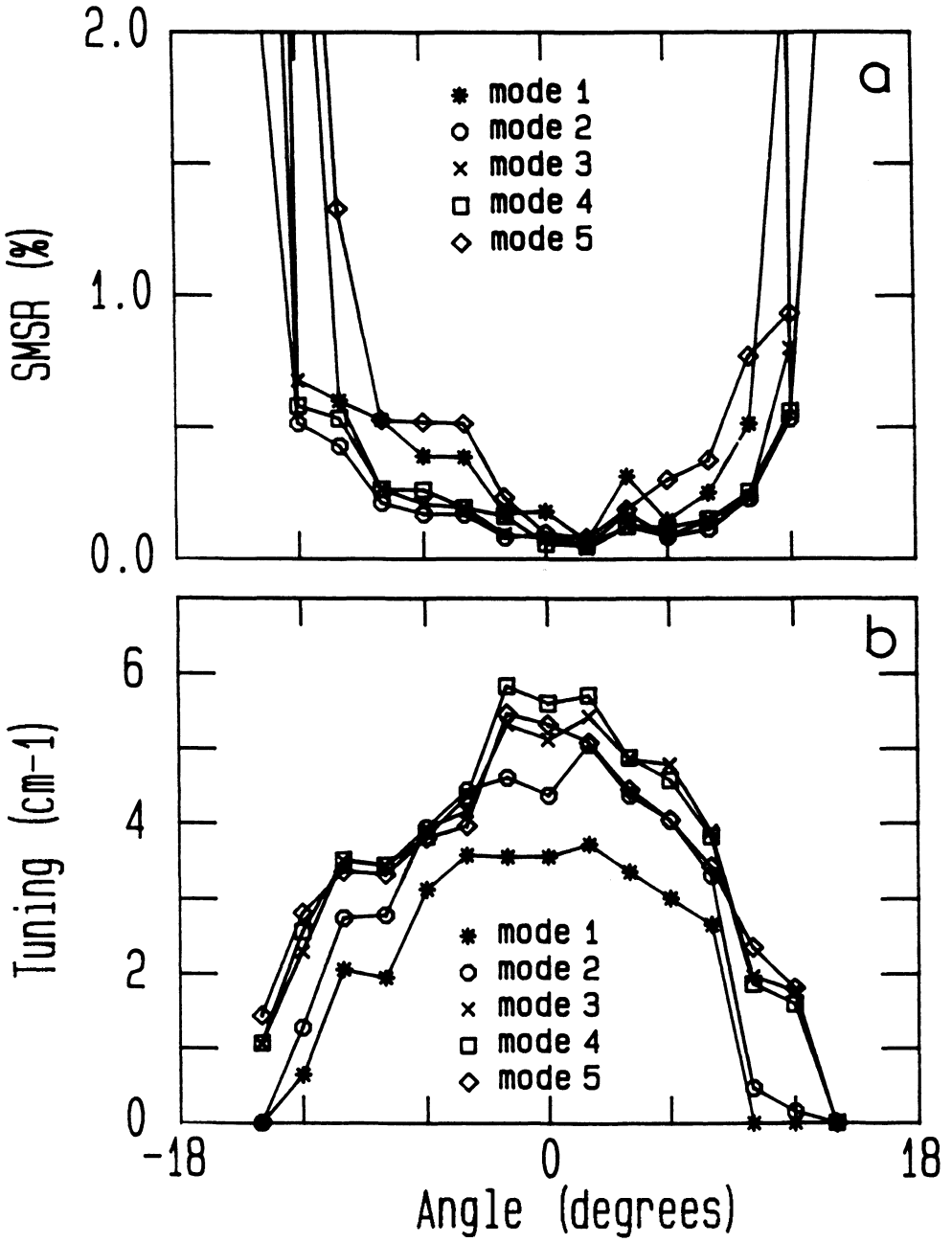

Figure 4–1: Plots of the (a) SMSR in % and (b) SM tuning range in cm^{-1} of an IRW laser as a function of a rotation of the external mirror.

The fact that the lowest SMSR value was not at θ=0 can be explained by the uncertainty in the SMSR which is discussed in the Discussion. As the mirror is rotated away from the normal position the SMSR increases and at $\pm 8^{\circ}$ the SMSR is $\leq$ 0.5 % (–23 dB). Note that the SMSR for the outer modes farthest from the gain peak increase faster. Past $\theta = \pm 8^{\circ}$ the SMSR rapidly increases until at $\theta \geq 12^{\circ}$ the laser is operating almost independently of the external cavity. The continuous SM tuning range is shown in Fig. 4.1b . At normal alignment the tuning range exceeds 5 cm^{-1} (0.85 nm) for three modes. The mode spacing was 5.25 cm^{-1} (0.89 nm) and thus 3 modes could be tuned almost a complete mode spacing giving complete spectral coverage of $\sim$ 15 cm^{-1} (2.7 nm). As the mirror is rotated away from the normal position the SM tuning range decreases until at $\theta \geq 12^{\circ}$ the laser is no longer SM. Near the normal position the tuning was limited on one side by threshold, and on the other by the limits of the current supply.

The SMSR and SM tuning can be related to the amount of optical feedback that was calculated in Chapter 2. At the normal position, SMSR of –33 dB and SM tuning ranges are found with feedback levels of 5×10^{-4} . When $\theta = 8^{\circ}$ the amount of feedback has reduced to 1×10^{-6} and the SMSR has risen to –(23–30) dB. The laser is no longer SM at $\theta = \pm 12^{\circ}$, and at this rotation the feedback is calculated to be $\leq 2 \times 10^{-7}$.

The similarity between the experimental (Fig. 4.1) and theoretical (Fig.2.5) results is apparent. The model predicts much better SMSR values ($\leq$ – 40dB)at normal alignment, but the trend is similar. The theoretical SM tuning results also follow the experimental trend although the theory shows somewhat lower SM tuning ranges. Thus one can conclude that the theoretical model is a reasonable representation of a SXC laser system. A quantitative comparison could

be attempted by matching the solitary laser model parameters to experiment and then add the feedback modification.

The SMSR and SM tuning range were also measured as a function of the external cavity length and the results are presented in Fig. 4.2 . Note that the SMSR increases for very short L. Even though the amount of optical feedback is large for short L, the SMSR is limited because the frequency selectivity , or Q, of the external cavity is reduced and modes adjacent to the main mode are also reinforced. As L increases, the SMSR reduces to levels of 0.1 % (–30 dB) and then increases for $L \geq 140$ μm. For these external cavity lengths the SMSR is limited not by the adjacent modes, but by modes that are separated from the main lasing mode by a multiple of the free spectral range of the external cavity. At these lengths the SMSR changes unpredictably with L since the SMSR depends on how well the external cavity modes are aligned with the laser cavity modes. The SM tuning as a function of L is shown in Fig 4.2b. The tuning is very small for $L \leq 40$ μm and is limited by the adjacent side modes which increase in energy due to the poor Q of the external cavity at short L, but the tuning rapidly increases with L to levels of $\geq$ 5 cm^{-1}. At L = 60 μm four of the six modes tuned more than a mode spacing. As L increases further, the SM tuning decreases because the amount of optical feedback is reduced and, more importantly, because other modes resonant with the external cavity begin to peak up.

To illustrate the potential of SXC lasers as tunable SM sources, the total single mode tuning range summed over all modes was measured as a function of L. Figure 5 shows the experimental results for an IRW laser. Trace A is the total spectral range covered by all the modes that could be forced to lase SM (the non–continuous SM tuning range). For example at L = 60 μm, 18 modes could be

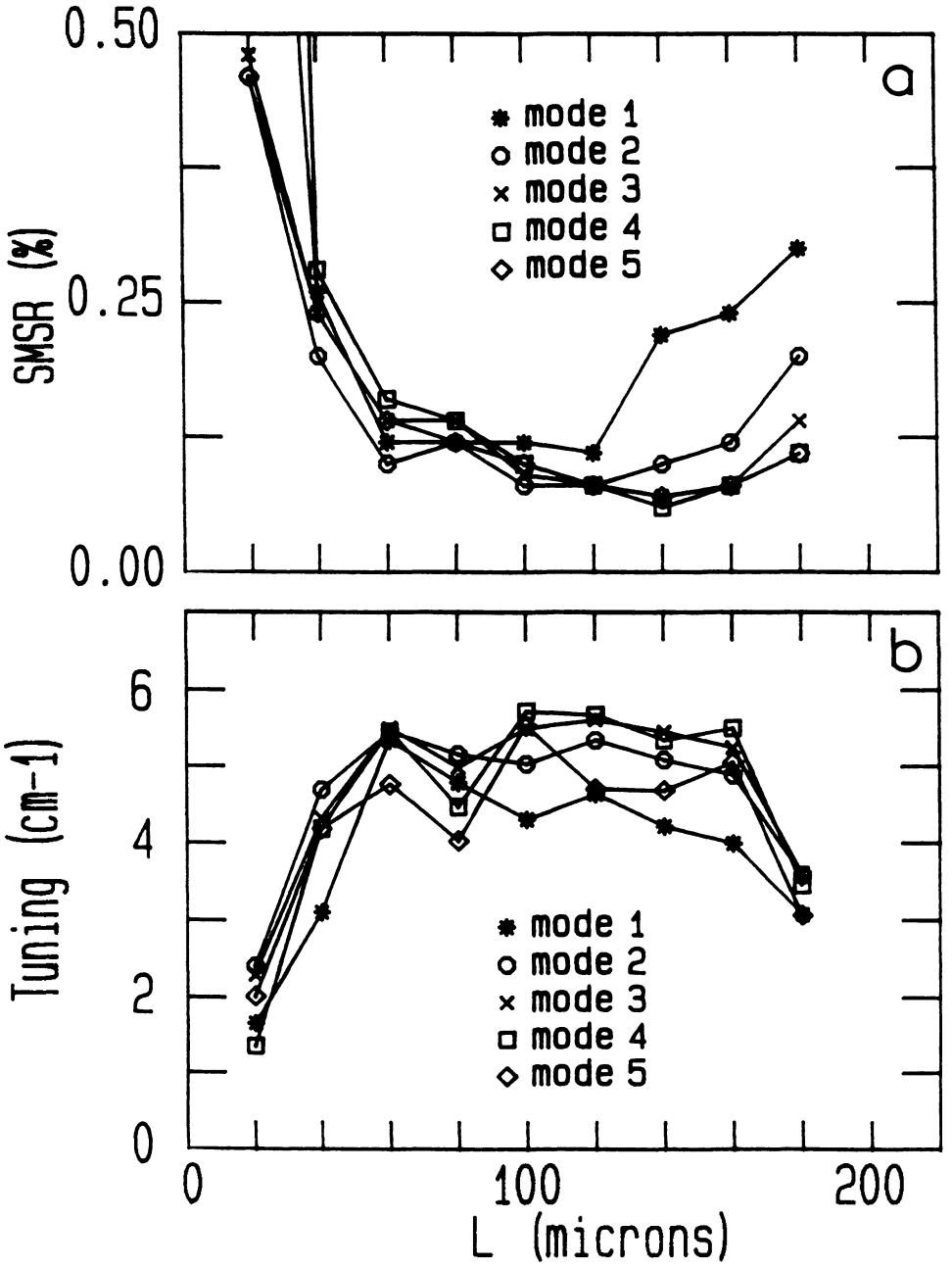

Figure 4–2: Plots of the (a) SMSR in % and (b) SM tuning range in cm^{-1} of an IRW laser as a function of the external cavity length.

forced to lase single mode. Trace B is the total continuous tuning range summed over all modes. At L = 60 μm the total continuous tuning range is measured to be 72 cm^{-1} of a possible 94 cm^{-1}, giving ~ 75 % spectral coverage. At this position 8 adjacent modes could be tuned greater than or equal to a mode spacing giving complete spectral coverage of 7.1 nm, or 42 cm^{-1}. The SM tuning range was limited by the adjacent modes for L $\leq$ 60 μm, but for L $\geq$ 60 μm the limiting factor was side modes resonant with the external cavity. The number of cavity modes that would lase SM increased as the external cavity length was shortened because of a larger amount of optical feedback coupling into the laser and a broadening of the free spectral range of the SXC.

For the SMSR and SM tuning range measurements, a second IRW laser made by the same manufacturer was found to produce qualitatively and quantitatively similar results.

The SMSR and SM tuning range results were found to be repeatable. For example the SMSR measurements, for L=160 μm and the mirror at the normal position, were found to have a standard deviation of ~30 % for modes 1–4 and increased to 80 % for mode 5 which was the mode farthest from the gain peak. This was the result for 12 separate measurements made over a four month period, with the laser being physically removed and replaced in the setup after the first six measurements. The standard deviation for the SMSR was found to increase with the rotation angle to ~50 % at θ=12. For L=160 μm and θ=0 the SM tuning range measurements were found to have a standard deviation of ~10 %. For all measurements the deviation was generally greater for modes farthest from the gain peak.

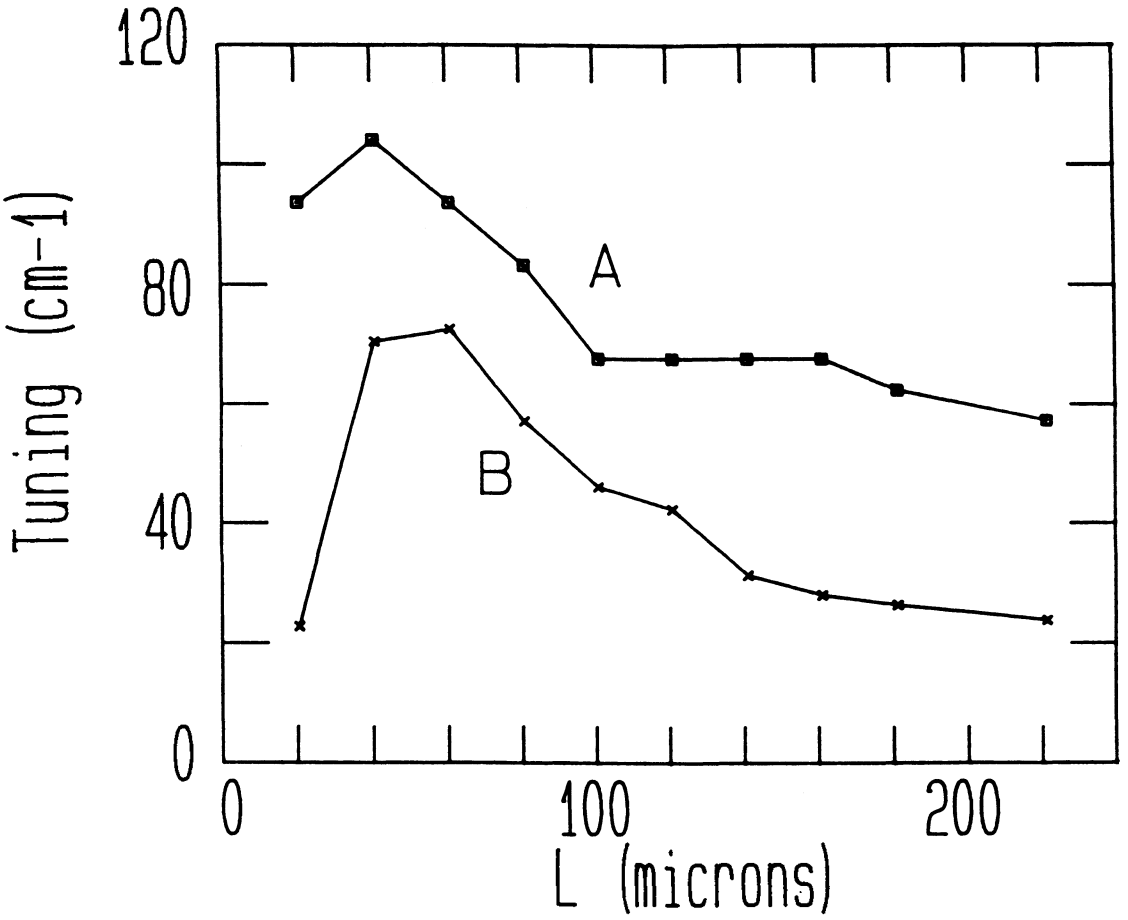

Figure 4–3: Trace of the total SM tuning range as a function of the external cavity length of an IRW laser where the SM tuning range is summed over all modes. Trace A shows the total spectral range covered by all modes that lase SM (non–continuous tuning range). Trace B shows the total spectral range covered by the continuous SM tuning range summed over all modes.

The standard deviations of all lasers tested were found to be of comparable magnitude and for the remaining laser types tested, these numbers are applicable.

4.2.2 gain guided lasers

The same set of measurements were performed on gain guided lasers. Figures 4.4 to 4.6 illustrate the results for a gain guided laser which exhibited the same qualitative trend as the IRW laser. Figure 4.4 shows the rotational experiments. The SMSR of the gain guided lasers were comparable to the IRW lasers and had a minimum SMSR of 0.06 % (–32 dB). Note that the SMSR of Fig. 4.4 increased at smaller rotation angles as compared to the IRW laser (see Fig.4.1). This behavior is somewhat surprising. Referring to the far fields and reflectivity plots (see Fig. 3.4 and 3.5) one can see that the calculated reflectivity falls off faster with angle for the gain guided laser. However the gain guided laser has side lobes that were smoothed over with the fitted Gaussians. Assuming that a better fit could be accomplished with angularly offsetted Gaussians one can conclude that the reflectivity would increase when the rotation coincided with these features. This behavior was not observed. The feedback level at the normal position was calculated to be 1×10^{-3}, almost twice that of the IRW laser. The SM tuning range for the gain guided laser reached a maximum of 3.5 cm^{-1} (0.6 nm) near normal alignment which corresponds to $\sim$ 70 % of a mode spacing. This is roughly a factor of two lower than the IRW laser. One problem in these measurements was the presence of self sustained pulsations (SSP) which limited the experimental tuning range. The current range was chosen to lie outside of SSP action to avoid

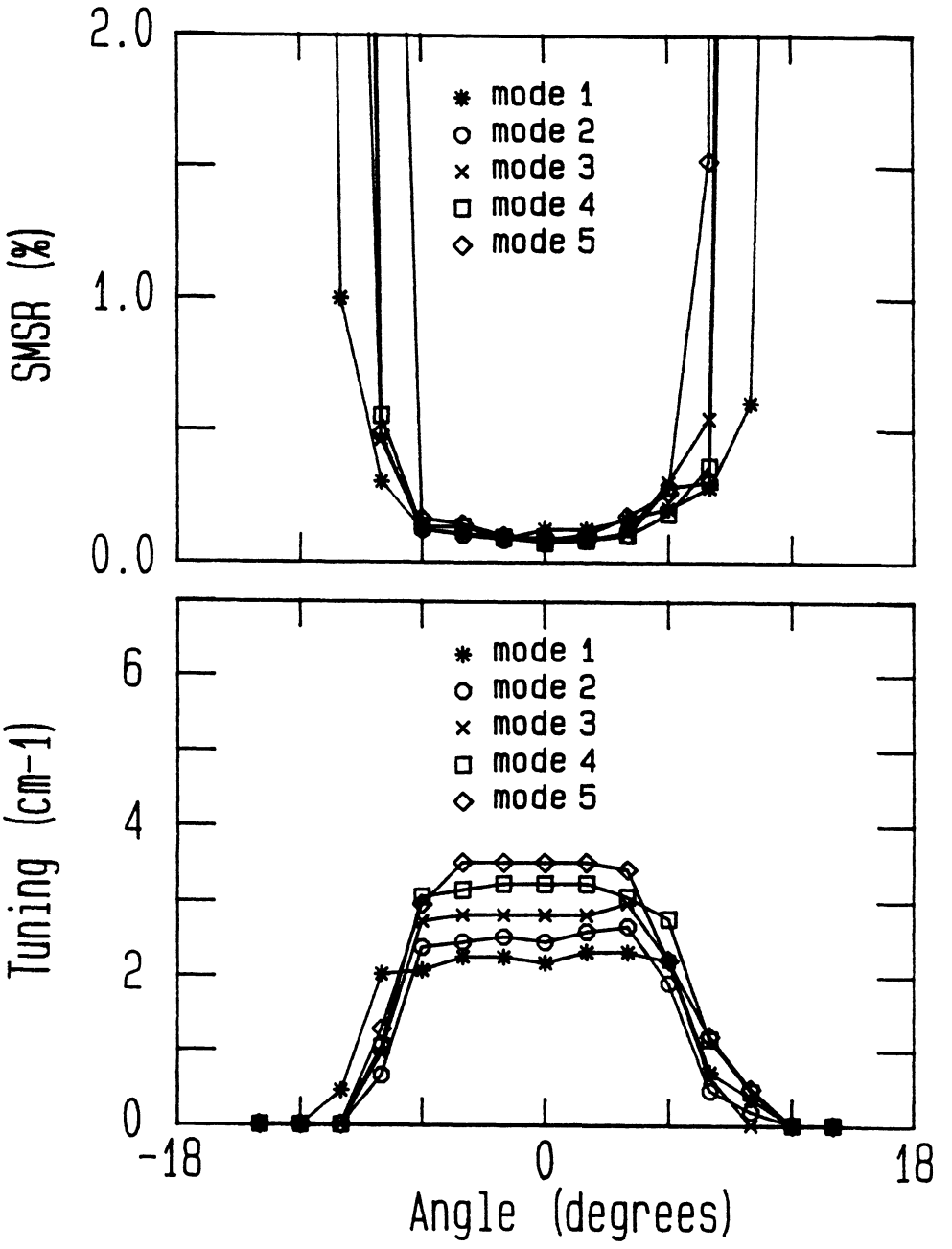

Figure 4–4: Plots of the (a) SMSR and (b) SM tuning range of a gain guided laser with respect to the rotation of the external mirror

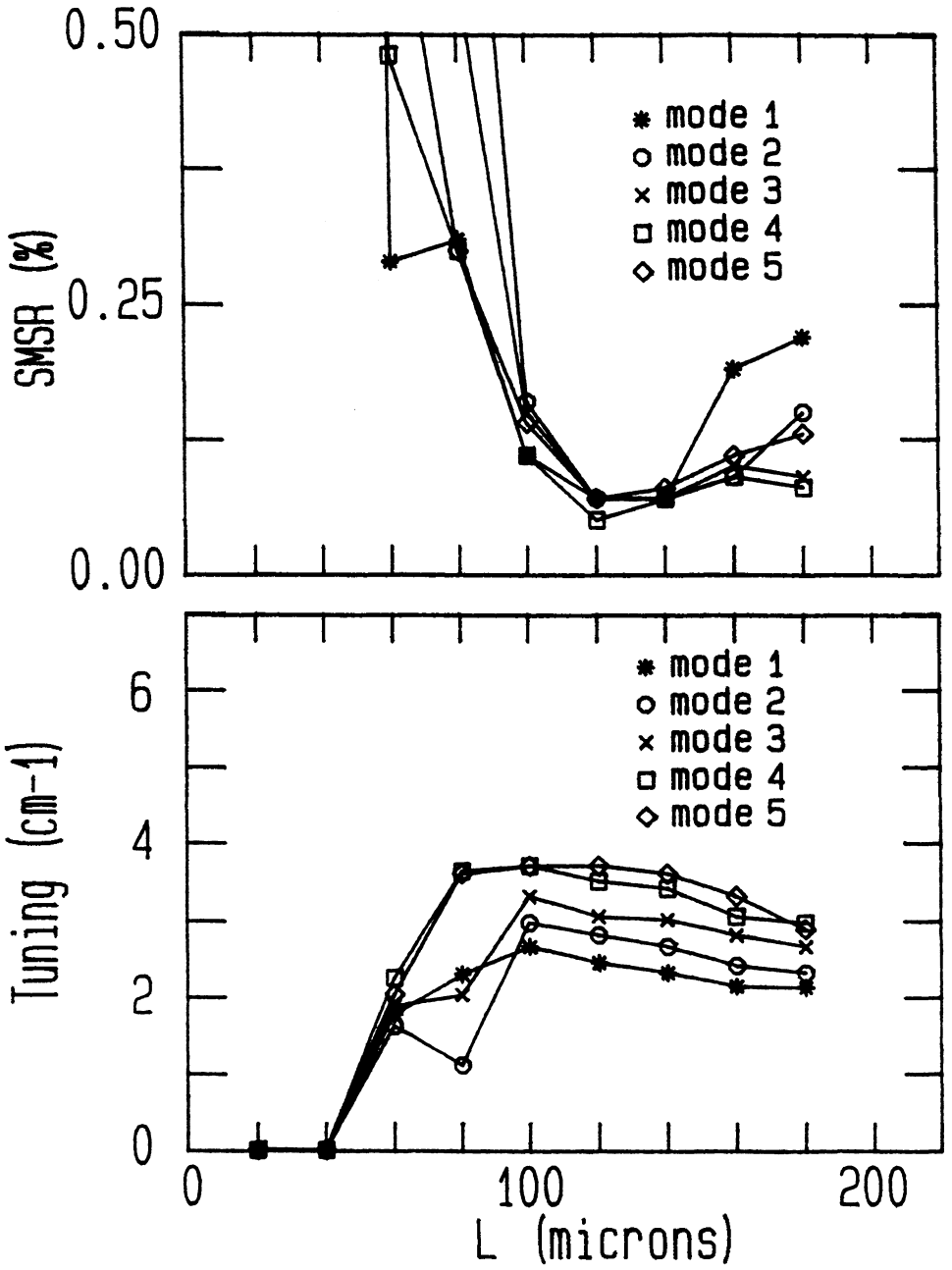

Figure 4–5: Plots of the (a) SMSR and (b) SM tuning range of a gain guided laser as a function of external cavity length.

this frequency instability. Unfortunately the SSP's occurred when the change in tuning with respect to the injection current was large which effectively closed out a large tuning region. Figure 4.5 shows the SMSR and SM tuning range versus L. Good SMSR values of $\leq$ 0.1 % were obtained only for L $\geq$ 100 μm. One would expect similar results as the IRW laser. The relative Q of the external cavity to the laser cavity is similar for the IRW and gain guided lasers since they both have the same laser cavity length. The SM tuning range as a function of L reached a maximum value of 3.8 cm^{-1} (0.64 nm). The total SM range of the gain guided laser mirrored the generally lower SM tuning ranges and is illustrated in Fig. 4.6 . The maximum total SM tuning range summed over all modes was 40 cm^{-1} which is 51 % of a 78 cm^{-1} wide spectral region. The maximum number of cavity modes that could be forced to lase SM was 11 at L = 60 μm.

A second gain guided laser made by the same manufacturer was found to exhibit qualitatively and quantitatively similar results.

4.2.3 buried heterostructure (BH) lasers

The SMSR results for the BH laser are illustrated in Fig. 4.7 . The SMSR values are presented for the 3 main modes, and show a minimum of 1.0 % (–20 dB) at normal alignment. Because of the fact that the SMSR was $\geq$ 1.0 % the experimental SM tuning ranges were insignificant, the best being 0.01 nm. The rotational far field for the BH laser was broader than the IRW and gain guided lasers, but the maximum feedback level of 3×10^{-4} was comparable.

The poor SMSR and SM tuning ranges can be explained by looking at the pumping level of the laser. For the SMSR experiments the laser current was set

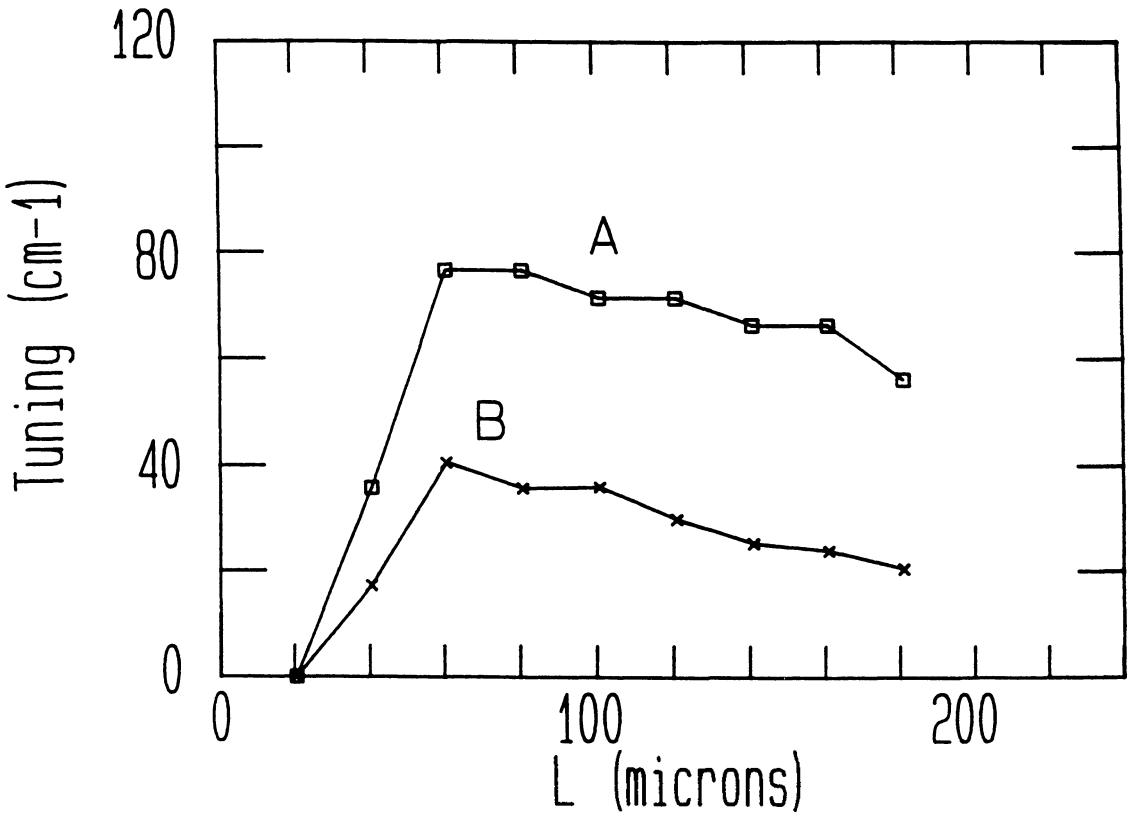

Figure 4–6: Total SM tuning range of a gain guided laser as a function of the external cavity length. Trace A shows the total non–continuous tuning range. Trace B shows the total SM tuning range summed over all modes.

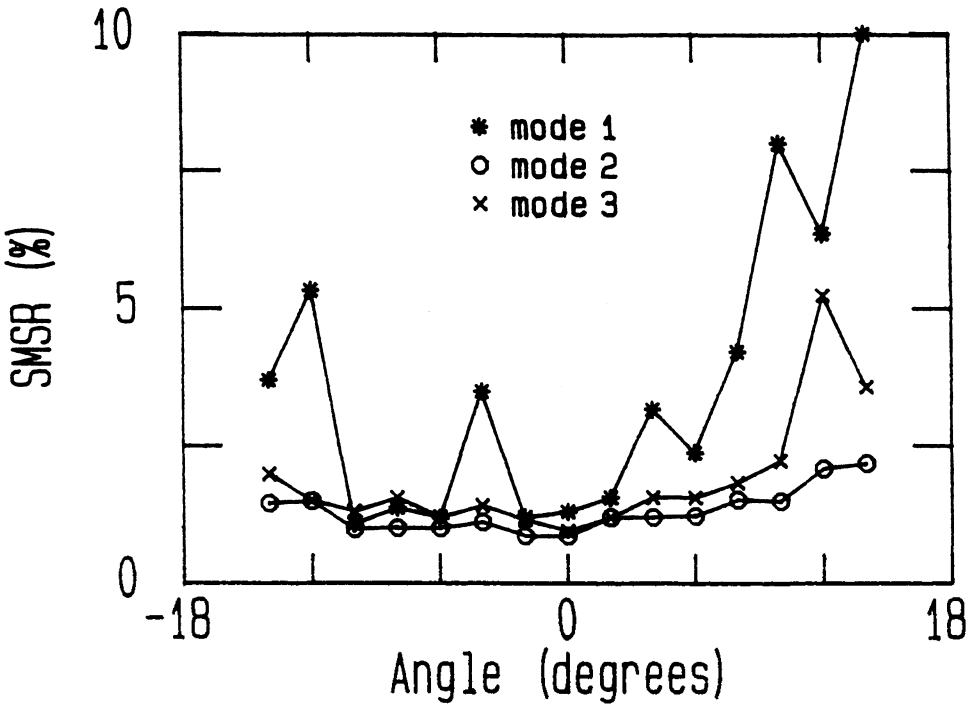

Figure 4–7: Plot of the SMSR of a BH laser as a function of the rotation of the external mirror.

to ~ 1.3 I_{th} . The gain guided and IRW lasers had threshold currents of ~ 100 mA, and thus the current was set to ~ 30 mA above threshold. The BH laser had a threshold of 20 mA, and thus the current was set to 6 mA above threshold. One must realize that it is the net gain of these devices that plays the crucial role in their above threshold performance, and therefore these devices should be compared at a similar net gain. This can be accomplished by operating all lasers at a specific current above threshold. The BH lasers were operating at only 6 mA above threshold compared to 30 mA for the gain guided and IRW lasers. Better SMSR were indeed found in measurements on one other short lived BH laser. At L = 160 μm and 10 mA above threshold the best SMSR was 0.32 % (–25 dB), a considerable improvement. This second laser was made by a different manufacturer.

Even with SMSR < 1.0 % the SM tuning range is expected to be small because the gain peak tuned 18 X faster than the cavity modes as compared to 8 X as fast for the IRW and gain guided lasers. The SM tuning range could be improved with an increased temperature shift provided by adjustment of the thermoelectric cooler/heater. This is generally true for all laser types, since in many cases the tuning was limited on one end by threshold.

4.2.4 0.76 μm GaAs laser (CSP)

The results for the GaAs laser are illustrated in Fig 4.8 and 4.9 . The SMSR and SM tuning range as a function of mirror rotation are illustrated in Fig. 4.8 . For these measurements L was set to 80 μm. The mode spacing for the 0.76 μm GaAs laser was measured to be 0.27 nm, or 4.75 cm^{-1}. The SMSR was relatively poor, having a minimum value of ~ 0.8 % near zero rotation. The

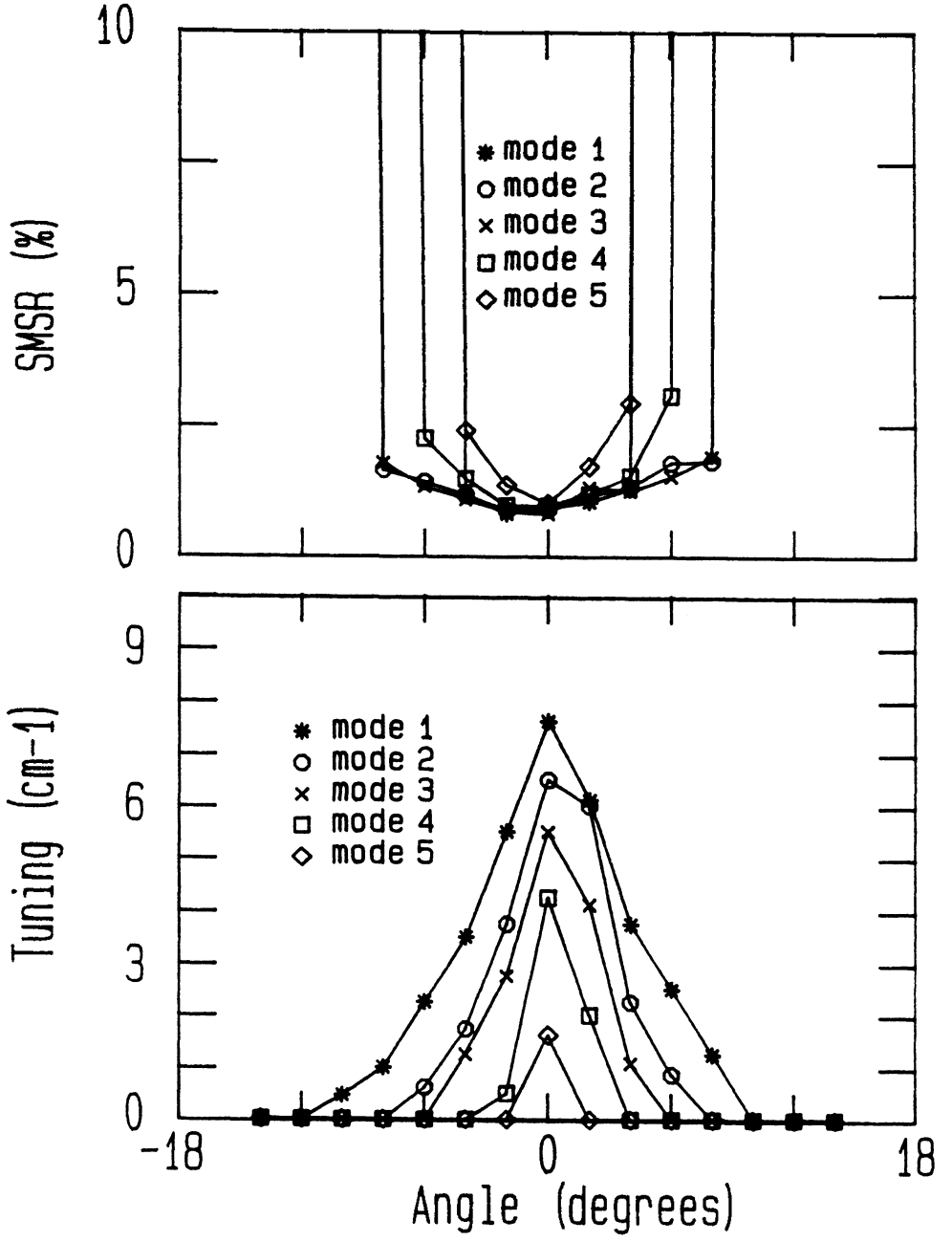

Figure 4.8: Plot of the (a) SMSR and (b) SM tuning range of a GaAs laser as a function of the rotation of the external mirror.

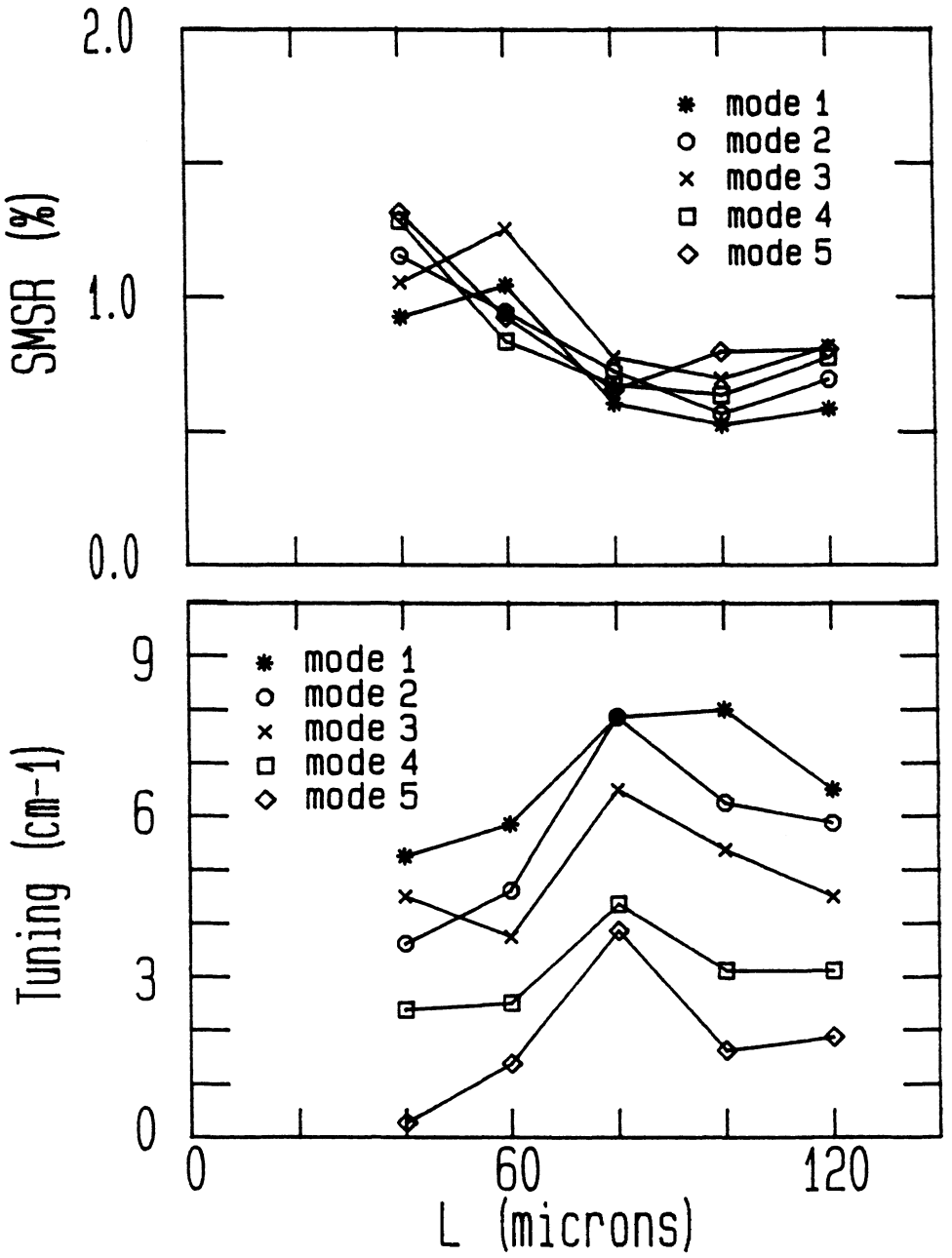

Figure 4–9: Plot of the (a) SMSR and (b) SM tuning range of a GaAs laser as a function of the external cavity length.

maximum SM tuning range was 7.6 cm^{-1} which for a 0.76 μm laser corresponds to 0.44 nm. The tuning range dramatically increased for longer wavelength modes. This is not surprising for GaAs lasers since they become more single mode as the driving current is increased. Without the external cavity the GaAs laser had most of its energy in only one mode for all significant injection currents above threshold. At $1.3 \times I_{th}$ the SMSR of the solitary GaAs laser was 2.8 % and the SMSR steadily decreased with current until at $2 \times I_{th}$ the SMSR was 0.7 %. The longer wavelength modes are centered in the gain at higher driving currents. Figure 4.9 shows the SMSR and SM tuning range as a function of external cavity length. The best SMSR was $\sim$ 0.5 % when L=100 μm. Larger external cavity lengths were not measured because the external mirror was stabilized by resting it on the laser mount platform which extended 120 μm beyond the laser facet. The SM tuning range as a function of L had a maximum value of 8 cm^{-1} (0.46 nm) at L=80 μm.

4.2.5 spherical mirrors

SXC lasers were also examined with a spherical reflector as the SXC element. Better performance is expected since the spherical mirror increases the amount of optical feedback due to its focusing properties. The phase fronts of the output beam are essentially spherical with a radius of curvature equal to L for L >> 0. The radius of curvature of the mirror was 200 μm, and thus at L = 200 μm the reflected beam is refocused back on the laser facet providing maximum feedback. The SMSR and SM tuning range as a function of L are presented in Fig. 4.10 for an IRW laser. The shortest L was 175 μm, and at this position the mirror was resting against the laser diode block which damped out mechanical vibrations. For L = 175

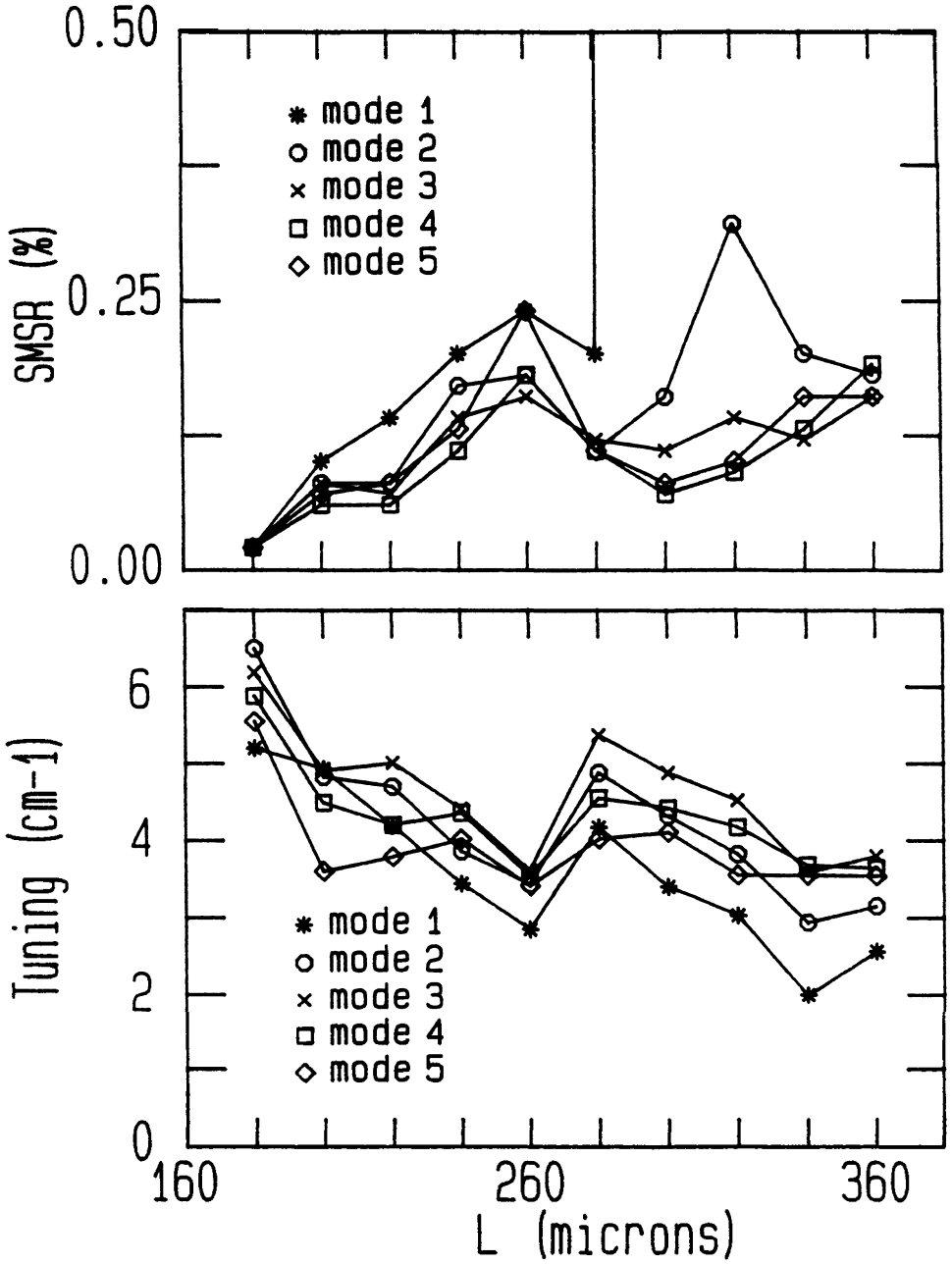

Figure 4–10: Plot of the (a) SMSR and (b) SM tuning range of an IRW laser as a function of the external cavity length using a spherical mirror as the SXC element.

μm the lowest SMSR was $\leq$ 0.02 % (–37 dB) and the SM tuning range was $\sim$ 6 cm^{-1} (1.01 nm). As L was increased the spherical mirror could not be well mechanically stabilized due to alignment constraints. Thus the SMSR and SM tuning ranges presented do not typify the expected results. As L increased the SMSR increased to $\geq$ 0.06 % (–33 dB) and the SM tuning decreased to $\leq$ 5 cm^{-1}. At L = 240 μm there is a local maximum in the SMSR and a local minimum in the SM tuning. At this position the limiting factor was side modes resonant with the external cavity. This behavior is not fully understood. If the beam is Guassian the maximum level of feedback should occur near 200 μm and decreases for L > 200 μm. With a spherical mirror secondary reflections can be significant. At the confocal position a secondary reflection would be $\sim$ 30 % of the first reflection. If the mirror was not perfectly aligned, multiple reflections do not necessarily add in phase which would degrade the resonant feedback.

The improvement that is expected with a spherical mirror is well illustrated in the results of the BH laser which are shown in Fig. 4.11 . The SMSR has been reduced to a minimum of 0.07 % (–31 dB) at L = 200 μm. The SM tuning range was a maximum of 0.54 cm^{-1} (0.1 nm) at L = 170 μm. Better tuning results of 0.5 nm have been found for anti–reflection coated BH lasers using an external grating to provide optical feedback [23]. The external grating provides large amounts of dispersive feedback . In this case the optical frequency was tuned by adjusting the heat sink temperature.

An interesting result is that the SM current tuning range had a maximum current of $\sim$ 50 mA (i.e. beyond 50 mA the SXC laser was not operating SM). This is 30 mA above threshold, similar to the SMSR measurements performed on the IRW and gain guided lasers. Thus at the same net pumping level above

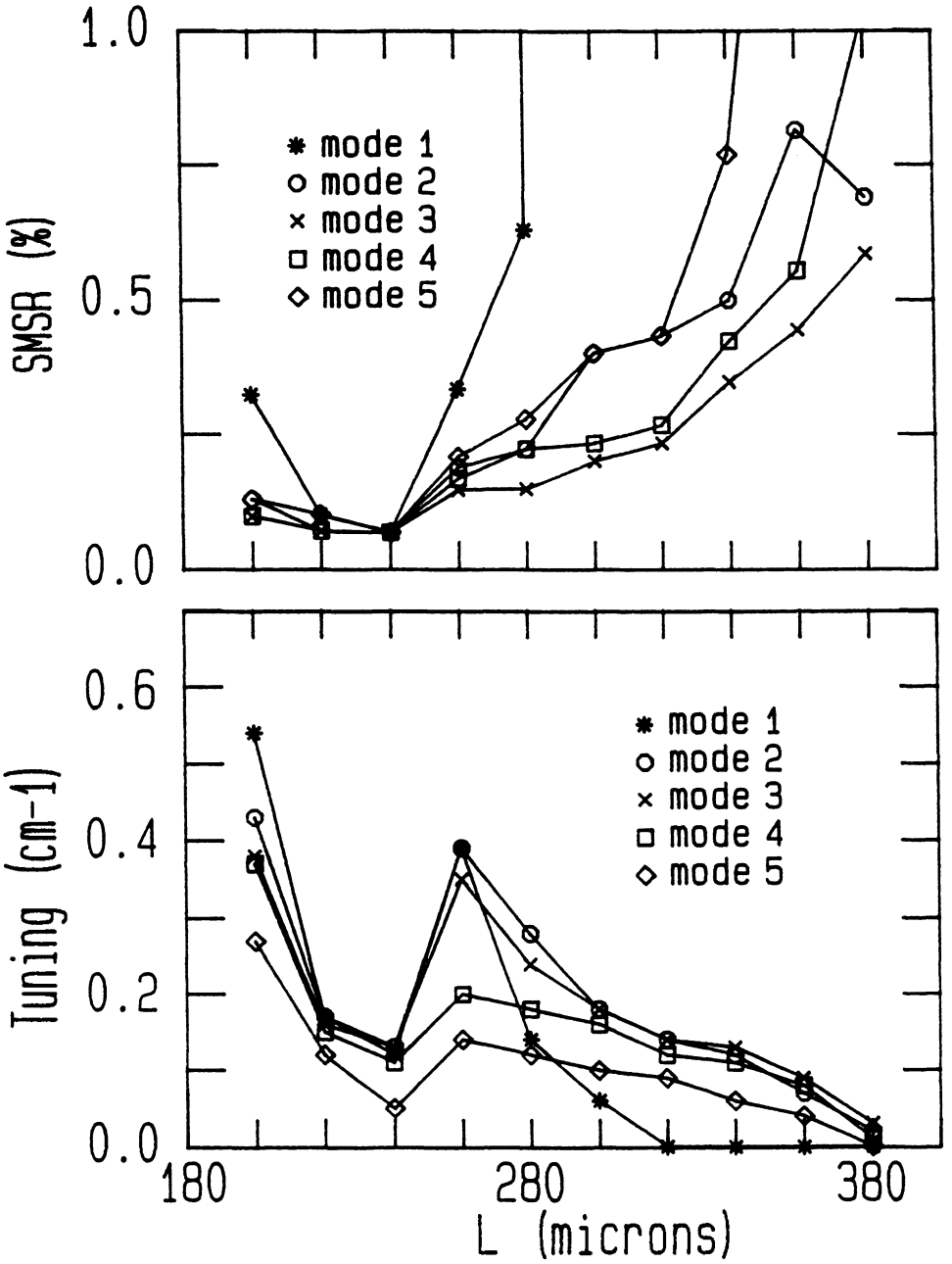

Figure 4.11: Plot of the (a) SMSR and (b) SM tuning range of a BH laser as a function of the external cavity length using a spherical mirror as the SXC element.

threshold the BH lasers have SMSR of > 1.0 %. This is much worse than the other laser types and it may be that device structure plays some role in determining the susceptibility to optical feedback. A second BH laser made by the same manufacturer was found to have similar results.

The spherical mirror could not be used with the GaAs laser because the laser was mounted on a heat sink platform which extended well beyond the feedback facet. The spherical mirror could therefore not be brought within a distance to provide reasonable amounts of optical feedback.

4.2.6 Discussion

There are several factors that seemed to affect the SMSR and SM tuning range. The lasers were mounted on heat sink blocks, and in some cases the top of the blocks extended out from the beneath the feedback facet. For these lasers the SMSR was found to depend very much on the tilt angle. It may be that reflections off the top of the heat sink were adding unwanted feedback. Also, the SMSR varied greatly as one repeatedly tuned L through the cavity modes (i.e. every $\lambda/2$). For a SXC laser consisting of an IRW laser and a spherical mirror at L=260 μm, a variation of 5 dB was found in the SMSR over 18 $\lambda/2$ cycles. Similar trends were noticed with planar mirror. These results may be due to the variation in surface quality of the reflector since the portion of the mirror that reflects light back to laser facet shifts as L is changed. For the planar mirror only an area of $< 2\ \mu m^2$ reflects light back to the laser facet and any small surface irregularity (i.e. dust particles) would severely alter the reflectivity. Multiple reflections may also contribute to the variation in the SMSR and is a more serious consideration for the

spherical mirror. But even for the planar mirror, a $1/2^{\circ}$ offset from the normal position would result in a secondary reflection of 7 % and a phase compared to the first reflection. The spherical mirror feeds back light from a much larger area and a poor surface would reduce the overall effective reflectivity due to phase mismatches.

Mechanical vibrations of the SXC element are another factor that limit the SMSR and SM tuning range. An IRW with a planar SXC element was found to have unstable SM output unless it was resting on a support bed. The mode would tend to mode hop to other adjacent resonant modes. This is an inherent design problem and such consideration should be taken when designing SXC modules.

One interesting note was found during the measurements of the SXC gain guided laser. It was found that the introduction of a SXC could eliminate the SSP's. The external feedback alters the single pass gain which effects the oscillation conditions of the laser cavity. This type of result indicates the possibility of using SXC's as a probing tool that perturbs or drastically changes the operating parameters of a diode laser. Indeed in the next section it will be shown how the SXC was used as a tool to probe the scattering/absorption loss of diode lasers.

4.3 Power/Voltage characteristics of SXC lasers

Several aspects of the power and voltage characteristics of SXC lasers were examined to gain additional insight to the operation of these devices. It is hoped that this information would lead to a broadening of their utility as single mode tunable sources.

Two effects were examined. One was the effect of a small modulation on the external cavity length. Previous studies have found that the output power of a SM SXC laser is slightly higher at single mode than at multimode [21]. This can easily be understood by examining the effective reflectivity. When the external cavity is optimized for SM operation R_{eff} is at a maximum, and similarly R_{eff} is a minimum at multimode operation. For a non–symmetrical resonator ($R_1 \neq R_2$) more light is emitted from the facet with lower reflectivity. Also, an increased overall reflectivity lowers the threshold current and thus increases the output power. It can be seen then that a small modulation to the external cavity length modulates the net reflectivity which in turn modulates the output power. By using a feedback loop the power modulation can be used to lock the external cavity at a length that produces SM output [21]. This technique was duplicated using the laser power and also attempted using the voltage across the laser terminals. A change in the output power is accompanied by a change in the laser voltage. A mode control technique utilizing the laser voltage releases any constraints on the output beam of the laser. This mode control ability is important since the external cavity length can change due to mechanical and thermal drift, and also because the external cavity resonance

shifts when the mode frequency is optically tuned.

The external differential quantum efficiency (DQE) , which is proportional to $\Delta P/\Delta I$ (P–power, I–current), was investigated with respect to the mode wavelength. To monitor the DQE the laser current was modulated at 1 kHz and the change in output power was measured. Simultaneously with the DQE, the accompanying voltage modulation across the laser diode was also measured.

A formulation for the DQE has been derived [32], and is given as

$$\eta_{ext} = \frac{\eta_{int}}{1 - \frac{2\alpha l}{\ln(R_1 R_2)}} \qquad 4.1$$

where η_{int} is the internal efficiency, α is the scattering/absorption loss, l is the laser cavity length, and R_i are the facet reflectivities. Equation 4.1 is numerically accurate for current levels reasonably above threshold such that the stimulated emission dominates and for output powers that are low enough such that power saturation of the gain does not occur. Beyond these limits the accuracy decays. For the DQE experiments the lasers were operated at $1.3 \times I_{th}$ and thus one can assume that (4.1) is numerically valid. Theoretical predictions [32,33] indicate that for the laser types used in this thesis (4.1) is a very good approximation.

The only wavelength dependent variables in (4.1) are the reflectivities and α. The reflectivity change for the wavelength range is insignificant and thus any significant change in the DQE as a function of wavelength can be attributed solely to α.

4.3.1 Application of a small modulation to L

For these measurements the nominal external cavity length was set to 160 μm. L was modulated by a 200 Hz 0.1 μm (peak–peak) sinusoid. This modulation amplitude was found to give maximum signal while maintaining stable single mode operation. The frequency was limited to $\leq$ 250 Hz by the response of the high voltage supply that controlled the PZT. The resultant power and voltage signals were then amplified and sent to a signal averager. An examination of the voltage signal is presented in Fig. 4.12 . The mode structures were monitored simultaneously with the voltage signals which are shown in the insets. Figure 4.12b shows the laser operating at optimum SM, and the voltage signal is relatively flat. When the external cavity length is de–optimized towards multimode output as shown in Fig 4.12a and 4.12c, the voltage signal acquires a modulation with a frequency that corresponds to the dither of L. Note the phase change as the laser oscillates multimode on the long wavelength side (Fig. 4.12a) to the short wavelength side (Fig. 4.12c). The peak to peak voltage at multimode was measured to be 30 μV. Similar types of signals were found monitoring the laser power, though the power modulations were of the opposite polarity. The voltage signals were particularly noisy and signal averaging was required to produce smooth traces. Higher dither frequencies would be preferred to get away from line noise.

It can be seen that these voltage signals can be used to control the external cavity length for SM output using standard feedback techniques. This procedure was in fact utilized to maintain optimum SM output as the optical frequency of a SM was current tuned through 3.5 cm^{-1} (0.56 nm) spectral range. It

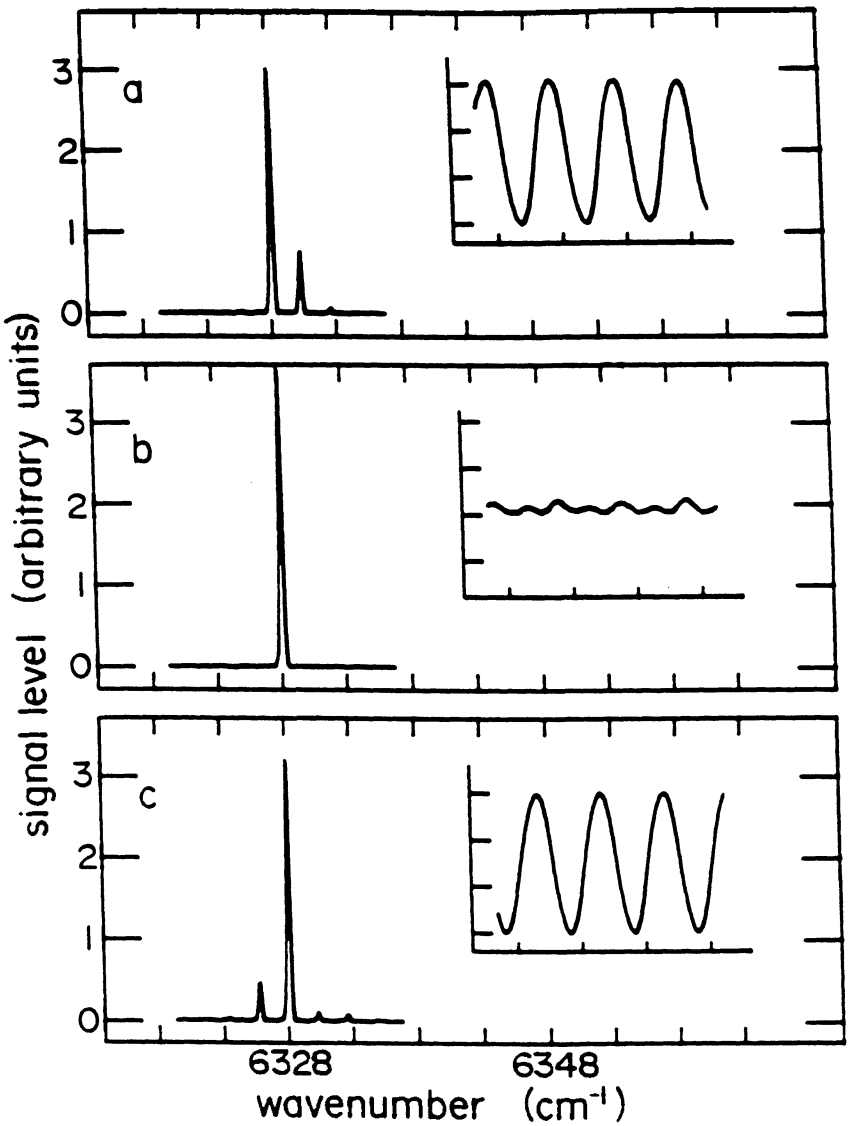

Figure 4–12: Plots of the output spectra and the voltage signals observed in controlling the laser mode. The inset traces show the voltage signal as a function of time. Plot (b) shows the modes and voltage signal when the external mirror is set for optimum SM output. Plots (a) and (c) show the modes and voltage signals when the external mirror is de–optimized to (a) shorter wavelength and (c) longer wavelength. Note the phase change of the voltage signal going from (a) to (c). The frquency of the voltage signals in (a) and (c) correspond to the dither frequency the external mirror.

was found that the mode control could maintain a SM for extended periods of time (> several hours) and would even guard against small vibrational perturbations. Each laser type exhibited similar power and voltage signals though the magnitude of the signals varied. The SXC laser can be locked to a SM by applying a small dither to L. It was desirable to determine how mode control affected the optical frequency of the SM laser. This was achieved by current tuning a controlled mode through an absorption line of CO_2 [25]. A modulation in $R_{eff}(L)$ will modulate the centerline mode frequency and this modulation will yield a derivative signal as the mode is tuned through an absorption line. The power transmission was synchronously detected with a lock–in amplifier set to the dither frequency. Figure 4.13a shows the directly measured CO_2 absorption line. The measured dither signal is plotted in Fig. 4.13b and shows the effect of the dither on the optical frequency. The path length of the absorption cell (24m) and the gas pressure (10 Torr) were known. The linewidth of the absorption was assumed to be Doppler broadened. Using this data the peak to peak frequency modulation of the mode was determined to be 160 MHz.

It is clear that mode control will add an unwanted modulation to any absorption measurements, and if derivative absorption detection techniques are used, it is desirable to use frequencies well beyond the dither frequency and its harmonics.

4.3.2 DQE measurements

The laser current of a SM SXC semiconductor diode laser was to $1.3 \times I_{th}$ and a 1 KHz small amplitude sinusoid was applied to the laser current which modulated the laser output power and the voltage across the laser diode. The

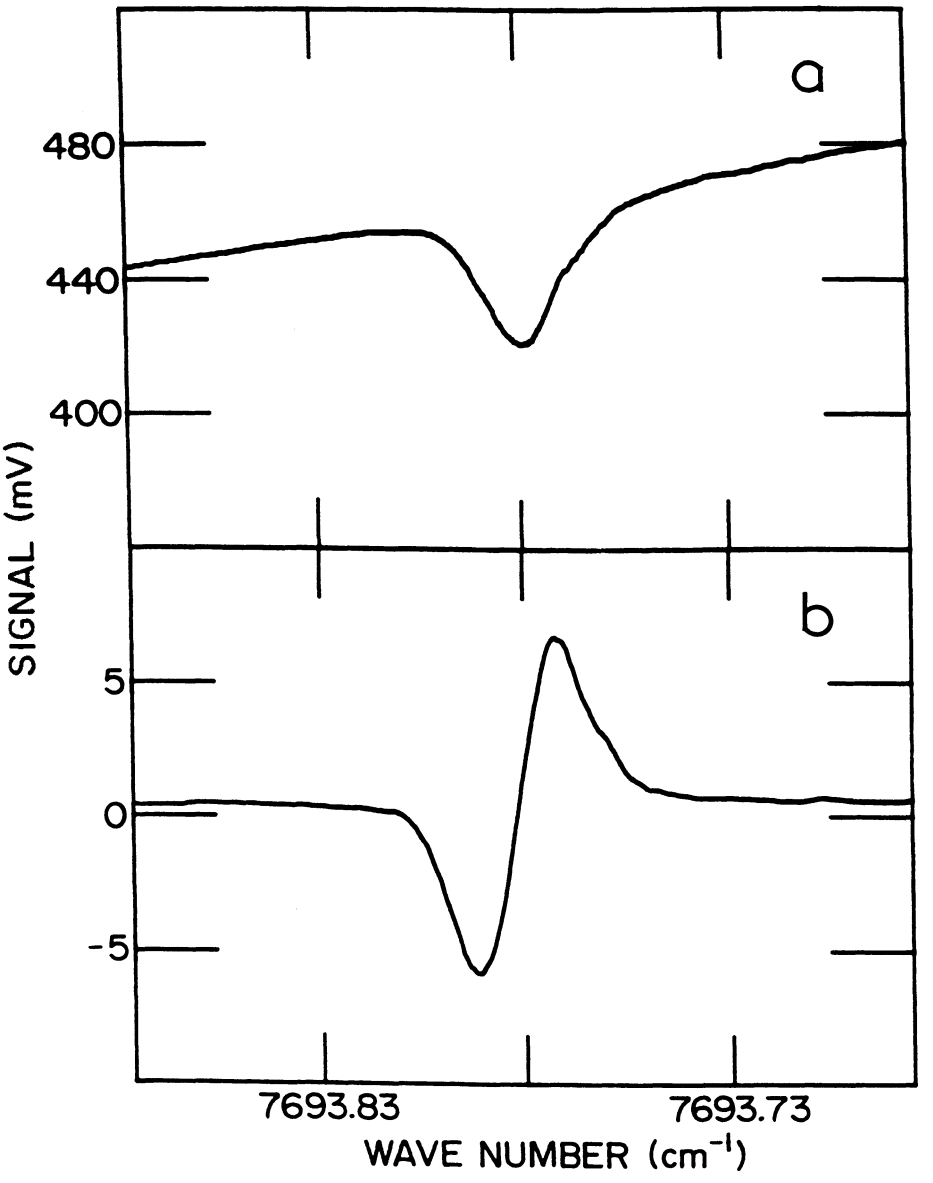

Figure 4–13: Plot of (a) the power transmission through an absorption line of CO_2 and (b) the transmission modulation amplitude caused by the modulation of the external cavity length.

modulated power, or DQE, and the modulated voltage across the laser terminals were detected synchronously using lock–in amplifiers.

As mentioned in Chapter 2 the DQE can be used to align the angular orientation of the external mirror. The measured 'DQE' is a sum of the output power from the front facet plus the contribution from the rear reflected beam which is partially transmitted through the InP cladding. Figure 4.14 shows the measured DQE as a function of rotation of an external planar mirror. The tilt angle was set to zero. The DQE peaks at zero rotation, and at this position the reflected beam axis will be along the output beam axis (assuming a symmetric laser) and thus will be most efficiently collected by the lens.

Considering the real DQE of the laser cavity only, the SXC increases the net reflectivity of the laser which increases the lasers DQE according to Eq. 4.1. This effect is masked by the presence of the reflected beam and thus a measure of R_{eff} by use of (4.1) is unattainable. However, the optical feedback also reduces the threshold current. A reduction in threshold shifts the Fermi levels of the semiconductor and therefore shifts the voltage across the diode. The modulated voltage was measured to detect this change as a function of mirror rotation (and hence optical feedback). The results were inconclusive due to noise and large drifts in the voltage signal. Improved electronics may result in conclusive findings.

To detect variations in the DQE and laser voltage modulations as a function of wavelength, the external cavity length was ramped linearly which caused the SM spectral output to be repeatedly tuned through the cavity modes. The modes were referenced to the measured trace by a second trace. For this reference trace 10% of the output beam was split off and sent to a monochromator which was calibrated to pass one mode only. Distinct variations in the DQE with respect to

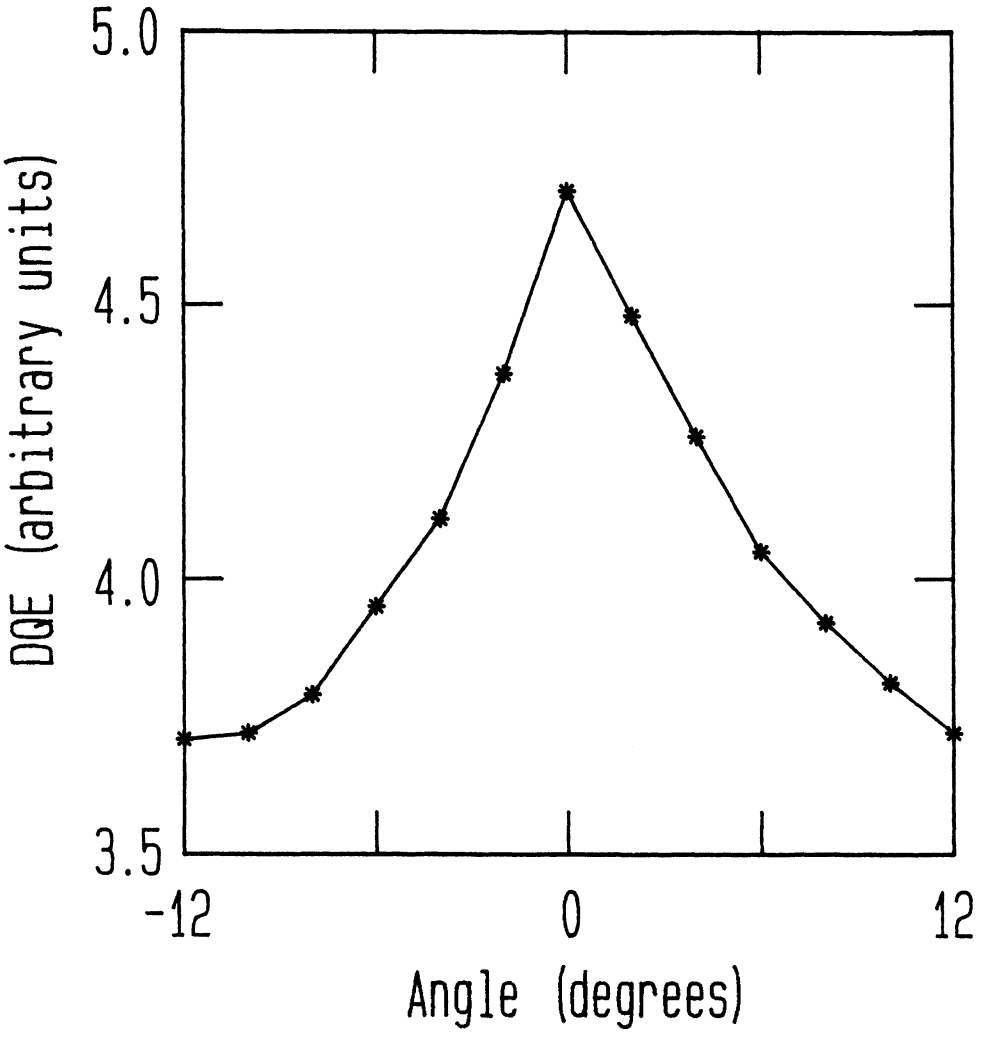

Figure 4–14: Plot of DQE as a function of rotation of the external mirror.

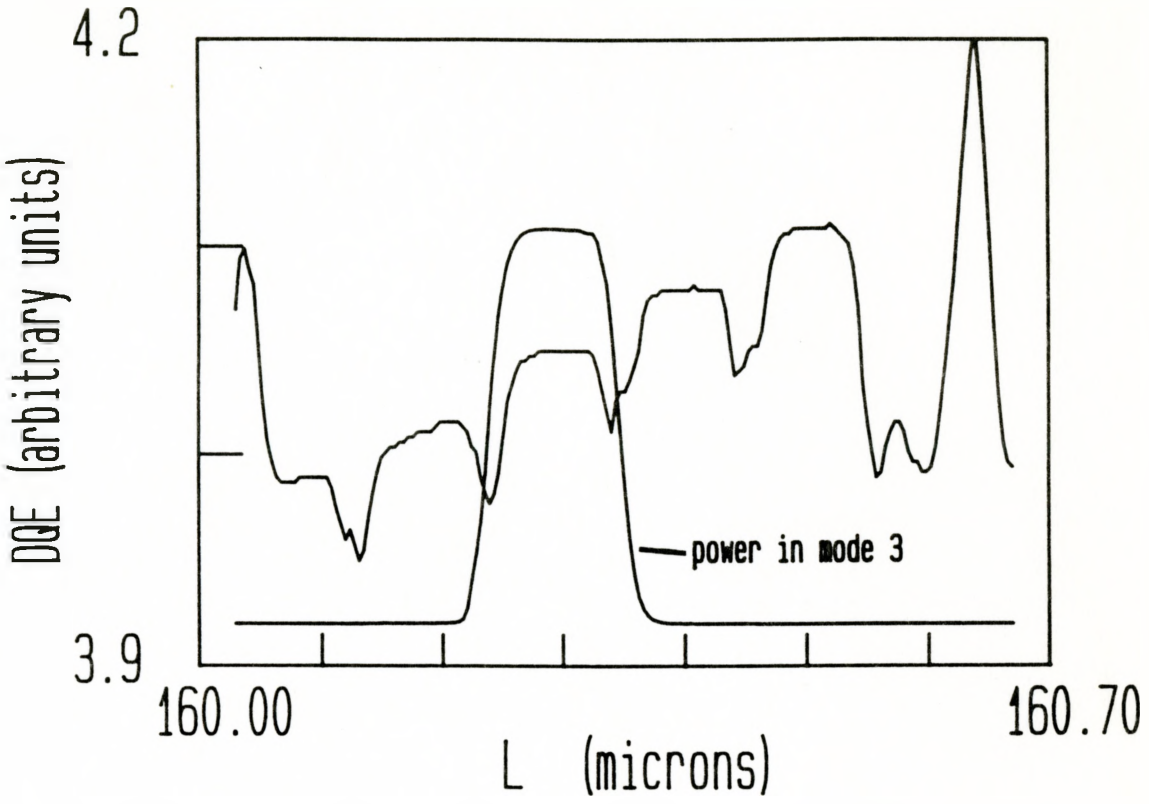

Figure 4–15: Trace of the DQE as a function of the external cavity length. The second trace shows the power in mode 3 as a function of the external cavity length.

wavelength were observed for all laser types. Figure 4.15 shows a plot of the DQE and the energy of mode 3 as L was linearly ramped which tuned the modes from short to long wavelength. For this trace the mirror rotation was offset from the normal position by 6° which gave good SM behavior and reduced the contribution from the reflected beam. The peak of the power in mode 3 aligns with a peak in the DQE trace and at the multimode points the DQE experiences a minimum. As the laser spectral output tunes from short to long wavelength the DQE increases. At the crossover point where the laser hops from the longest wavelength mode to the shortest wavelength mode many modes oscillate and the DQE experiences a sharp peak. The shape of the trace repeats itself as L cycles through the modes (every $\lambda/2$). Qualitatively similar results were found when the SXC geometry was altered (tilt,rotate,L) and the feedback level changed. Major differences seemed to occur when the mode composition of a mode hop changed. For the trace in Fig. 4.15 only the adjacent side modes were involved in a SM mode hop. The shape of the DQE with respect to wavelength may be explained by the frequency dependence of the absorption/scattering loss term α of Eq. 4.1 . It is known that the loss of InGaAsP materials decreases with wavelength [34]. A similar trend has been found for GaAs BH lasers with the rate of change α with respect to λ estimated to be $0.5\ \mathrm{cm}^{-1}/\ \mathring{\mathrm{A}}$ [35].

The DQE was measured for a solitary multimode IRW laser using a calibrated detector and found to be 0.14 A/W . This was for an injection current that had mode 1 as the central mode. This average value for the DQE was assigned to mode 1 of Fig. 4.4 . The loss of the other wavelength modes were normalized by the DQE of mode 1 using the data of Fig. 4.4 and Eq. 4.1 . The resultant loss versus wavelength trace is illustrated in Fig. 4.16 . The slope of the trace is

estimated to be 3.2 $cm^{-1}/\AA$ which is a factor of 6 greater than that found for GaAs lasers in Ref. [35]. The calculation was corrected to account for the detector response. The DQE was measured for the gain guided and BH lasers and the result is illustrated in Fig. 4.17 . A similar trend is observed as for the IRW laser. The magnitude of the changes in the DQE traces suggest that the absorbtion coefficient of the gain guided laser changes more rapidly with wavelength than the IRW laser and the reverse for the BH laser. Note the presence of side modes in the power trace of Fig. 4.17a and 4.17b . When the cavity mode tuned from long to short wavelength the DQE was dramatically increased. The reason for this is not clear. Generally when tuning from long to short wavelength, many modes were involved in the mode hop .

The voltage modulation was detected simultaneously with the DQE and both traces are shown in Fig 4.18 as a function of L. As the lasing mode tunes to longer wavelength the voltage modulation shows the opposite trend to the DQE. This can be explained by considering the Fermi levels. As the mode tunes to longer wavelength the loss decreases which reduces the threshold current. The inversion necessary to maintain laser oscillation is reduced and therefore the Fermi levels are lowered. This reduces the voltage across the laser diode.

The shape of the voltage trace repeated as the modes cycled every $\lambda/2$. It is possible to map the mode to the voltage trace provided by changing L. By monitoring the corresponding PZT voltage, L can be changed to select a particular mode. The calibration can be repeated at any time to compensate for thermal or mechanical drift of L. Thus the mode of a SXC SM laser can be known simply by relating the laser voltage trace to the PZT voltage which controls L. The actual wavelength of each mode need be calibrated only once using a monochromator.

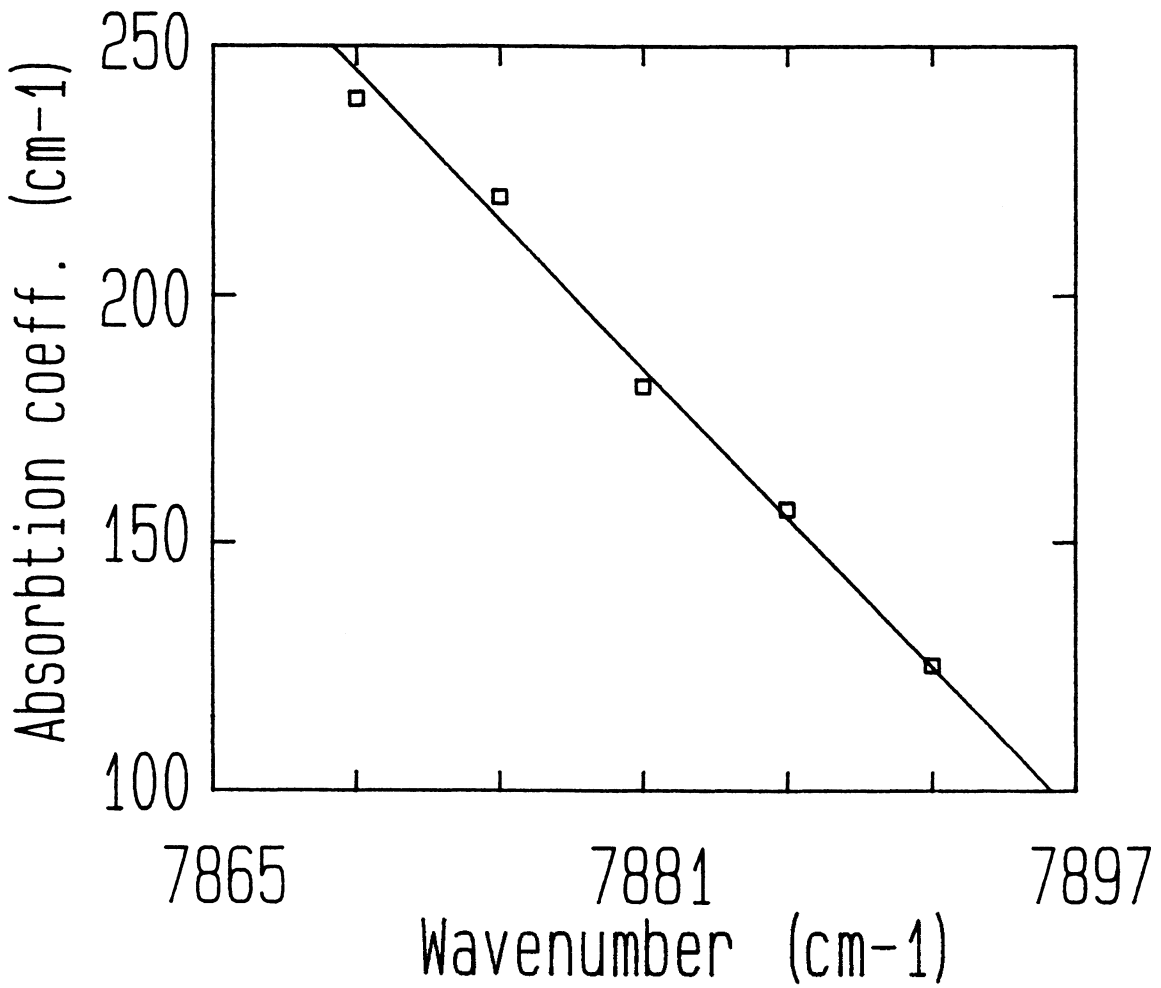

Figure 4–16: Trace of the calculated absorption coefficient of an IRW laser as a function of wavelength.

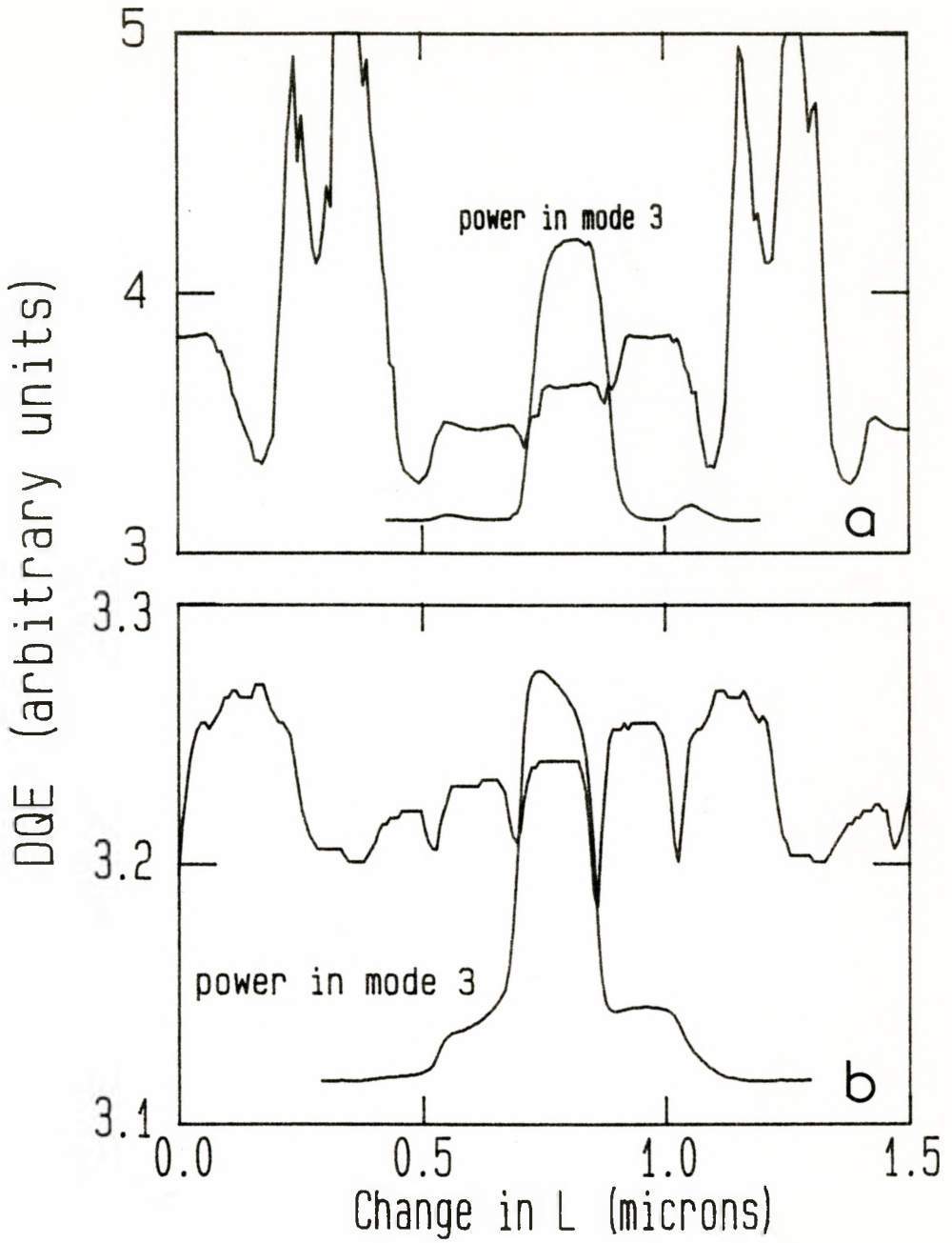

Figure 4–17: Trace of the DQE as a function of the external cavity length for a (a) gain guided laser and a (b) BH laser. Each plot is accompanied by a trace of the power in mode 3 as a function of the external cavity length.

This gives a crude estimation of the lasing wavelength. A finer estimation can be realized by characterizing the laser wavelength with respect to the operating temperature.

4.4 Summary

The SMSR and SM tuning range were measured for various SXC laser and reflector configurations. For an IRW laser with a planar SXC the SMSR could be reduced to –33 dB and the maximum SM tuning range was 6 cm^{-1} (1.01 nm). IRW lasers showed the best overall results of the lasers examined. Gain guided lasers showed similar SMSR of –32 dB, but the largest SM tuning range was was 4 cm^{-1}. This limit was largely due to the presence of SSP's which limited the current range. With planar SXC elements the BH lasers had poor SMSR values of $\geq$ –20 dB. It is reasoned that the driving current was set too low for optimum results. Higher driving currents on a different BH laser produced SMSR values of –26 dB. The GaAs laser had a minimum SMSR of 0.5 % and a maximum SM tuning range of 8 cm^{-1} (0.46 nm).

The best SMSR and SM tuning range values were found when the external mirror was aligned at, or near, the normal position. For the IRW and gain guided lasers, external cavity lengths of $\sim$ 120 μm give low SMSR values and large SM tuning ranges. The SMSR and SM tuning range were reasonably insensitive to small angular alignment deviations of $\pm$ 2–4°. The GaAs laser was more sensitive to angular alignment deviations and the SMSR and SM tuning range degraded substantially for a $\pm$ 2° change.

The use of spherical mirrors could improve the performance significantly,

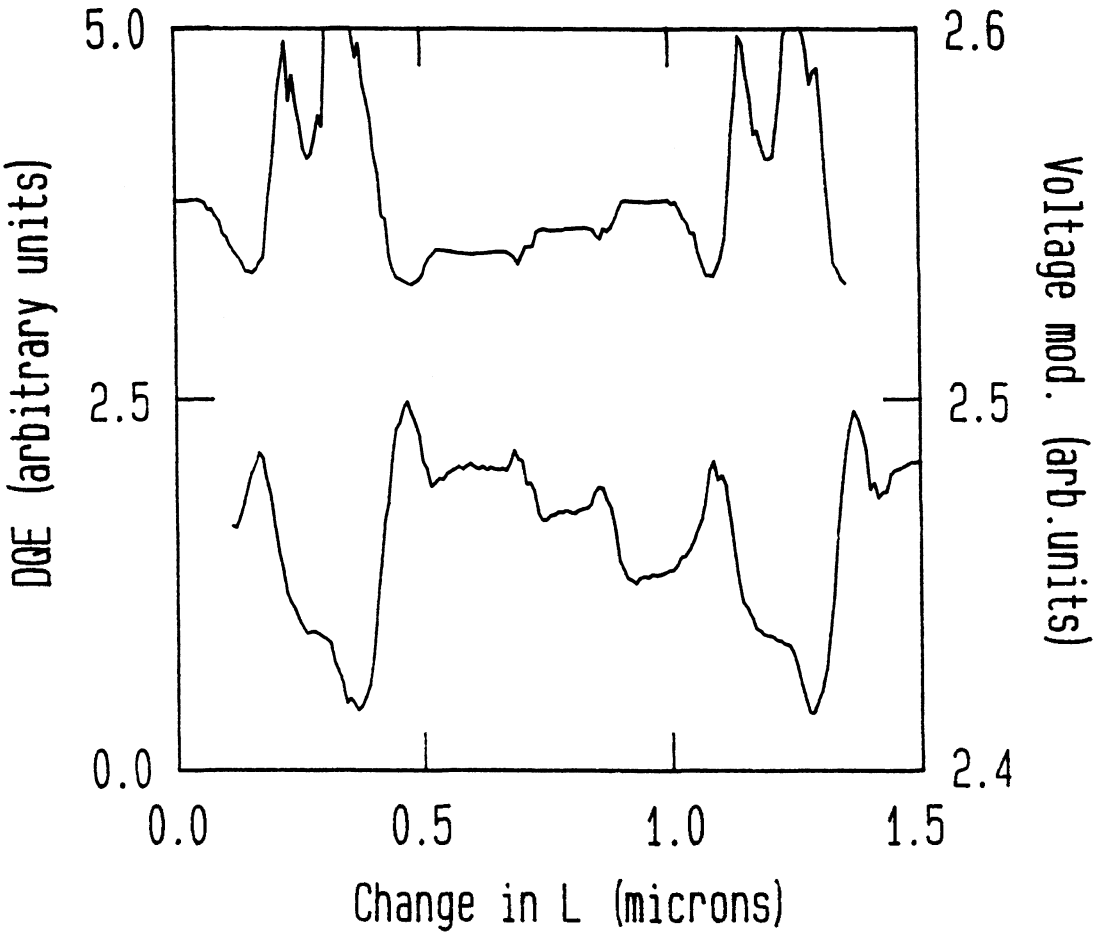

Figure 4–18: Trace of the DQE and the amplitude of the laser voltage modulation as a function of the external cavity length. Trace A shows the DQE and trace B shows the amplitude of the voltage modulation. Note the inverted trend of the voltage modulation as compared to the DQE.

and optimum results require mechanical stabilization of the mirror. For the IRW laser SMSR of –37 dB and a maximum SM tuning ranges of 6.4 cm^{-1} (1.1 nm) were found at L = 175 μm and the mirror stabilized. The BH laser had SMSR of –31 dB and a maximum SM tuning range of 0.54 cm^{-1} (0.1 nm).

Several aspects of the laser power and voltage were examined. It was found that the power and voltage signals that resulted from a small modulation in the external cavity length L, could be used to control L for optimum single mode output. Thus L can be automatically adjusted to compensate for mechanical and thermal drift, and for tuning of the optical frequency.

The external differential quantum efficiency (DQE) was found to increase with wavelength and this trait was attributed to the wavelength dependence of the scattering/absorption loss, α . The rate of change of α as a function of wavelength was determined to be 3.2 cm^{-1}/ Å for IRW lasers. Qualitatively similar results were found for gain guided and BH lasers although the magnitude of the change in the DQE as a function of wavelength was found to be larger for gain guided lasers and smaller for BH lasers as compared to IRW lasers.

CHAPTER 5

CONCLUSIONS

Short external cavity (SXC) semiconductor diode lasers were investigated for use as single longitudinal mode (SM) tunable sources. The side mode suppression ratio (SMSR) and the SM tuning range were measured with respect to a) external cavity length and b) angular orientation of the SXC element. Measurements were performed on two gain guided, two inverted rib waveguide (IRW) and two buried heterostructure (BH) 1.3 μm lasers and a 0.76 μm BH GaAs laser. Planar and spherical mirrors were used as the SXC element.

With a planar mirror the IRW lasers showed the best overall promise as single mode tunable sources. The minimum SMSR was –33 dB and the SM tuning range reached a maximum of 6.0 cm^{-1} (1.01 μm). Gain guided lasers also showed good results having very good SMSR (–32 dB) and reasonable SM tuning ranges (4 cm^{-1}). The main drawback with using gain guided lasers was the presence of self sustained pulsations (SSP) which limited the tuning ranges. The BH lasers exhibited poor results with a minimum SMSR of –23 dB and SM tuning ranges of $\leq$ 0.01 nm . The total SM tuning range summed over all modes was found to be 72 cm^{-1} of a possible 94 cm^{-1}. This was the result with an IRW laser and an external cavity length, L, equal to 60 μm . At this position 8 modes could be tuned greater than or equal to a mode spacing, giving complete spectral coverage of 42 cm^{-1} (7.1 nm).

The best SMSR and SM tuning range values were found when the external mirror was aligned at, or near, the normal position. For the IRW and gain

guided lasers, external cavity lengths of $\sim$ 120 μm give low SMSR values and large SM tuning ranges. Greater spectral coverage for the total SM tuning range summed over all modes is found for external cavity lengths of $\sim$ 60 μm but at the expense of larger SMSR values. The SMSR and SM tuning range were reasonably insensitive to small angular alignment deviations of $\pm$ 2–4°. The GaAs laser was more sensitive to angular alignment deviations and the SMSR and SM tuning range degraded substantially for a $\pm$ 2° change.

A spherical mirror could improve the performance of SXC lasers. With a spherical mirror , the SMSR of an IRW laser was $\leq$ –37 dB and the SM tuning range was $\geq$ 6 cm^{-1}. The performance of the BH laser was dramatically improved with a sperical mirror. The SMSR reduced to –30 dB and the SM tuning range was 0.5 cm^{-1} (0.1 nm) .

The best performance for all laser types was found when the external cavity element was aligned at the normal position (parallel to plane of the laser facet) and the level of optical feedback was maximized. External cavity lengths of $\leq$ 100 μm give good SMSR and large SM tuning ranges.

The power and voltage characteristics of SXC lasers can be utilized to increase their utility as SM tunable sources. A method of controlling the laser SM using the voltage signals resulting from a small modulation of L was discovered. The modulation of L also modulated the centerline frequency of the lasing mode ($\simeq$ 160 MHz peak–peak). The external differential quantum efficiency (DQE) was found to increase with the lasing wavelength, and this phenomenon was explained by the wavelength dependence of the absorption/scattering loss α . The rate of change of α as a function of wavelength was found to be 3.2 cm^{-1}/Å for IRW lasers. Qualitatively similar results were observed for gain guided and BH lasers.

The work reported on in this thesis can be continued in several directions. The A.C. response of SXC lasers can be studied to determine the feasibility of SXC lasers as sources in optical communication systems. The linewidth effects of a SXC on a diode laser are not well known and it may be possible to significantly narrow the linewidth with a well aligned SXC. The large non–continuous tuning range of SXC lasers may be utilized to probe the gain as a function of wavelength and perhaps be employed to search for evidence of hole burning.

APPENDIX

The level of optical feedback is found by calculating the coupling efficiency between the output beam at the laser facet, and the evolved reflected beam. The geometry of the SXC element is shown in Fig. A.1 for a rotation in the xz plane. The center of the laser mode is defined at O. The beam emitted from the laser facet reflects off the external mirror and the center of the reflected beam is at position O' when it interacts with the laser facet. The transformation from the O to the O' coordinate system is given by

$$x' = -z\sin 2\theta + x\cos 2\theta + L\sin 2\theta \tag{1}$$

$$z' = z\cos 2\theta + x\sin 2\theta \tag{2}$$

where θ is defined as the rotation angle between the the beam axis and the normal to the external mirror face. The beam is assumed to be Gaussian and can be decoupled into separate components

$$E(x,y,z) = E_x(x,z)\, E_y(y,z) \tag{3}$$

with the normalized E_x component described by [36]

$$E_x(x,z)=\left(\frac{2}{\pi}\right)^{1/4} \frac{1}{\sqrt{\omega_x}} \exp\left[\frac{-x^2}{\omega_x^2} \right] \exp\left[-i\left(kz + \frac{\pi x^2}{\lambda R_x} - \arctan\left(\frac{\lambda z}{\pi \omega_{ox}^2}\right)\right)\right] \tag{4}$$

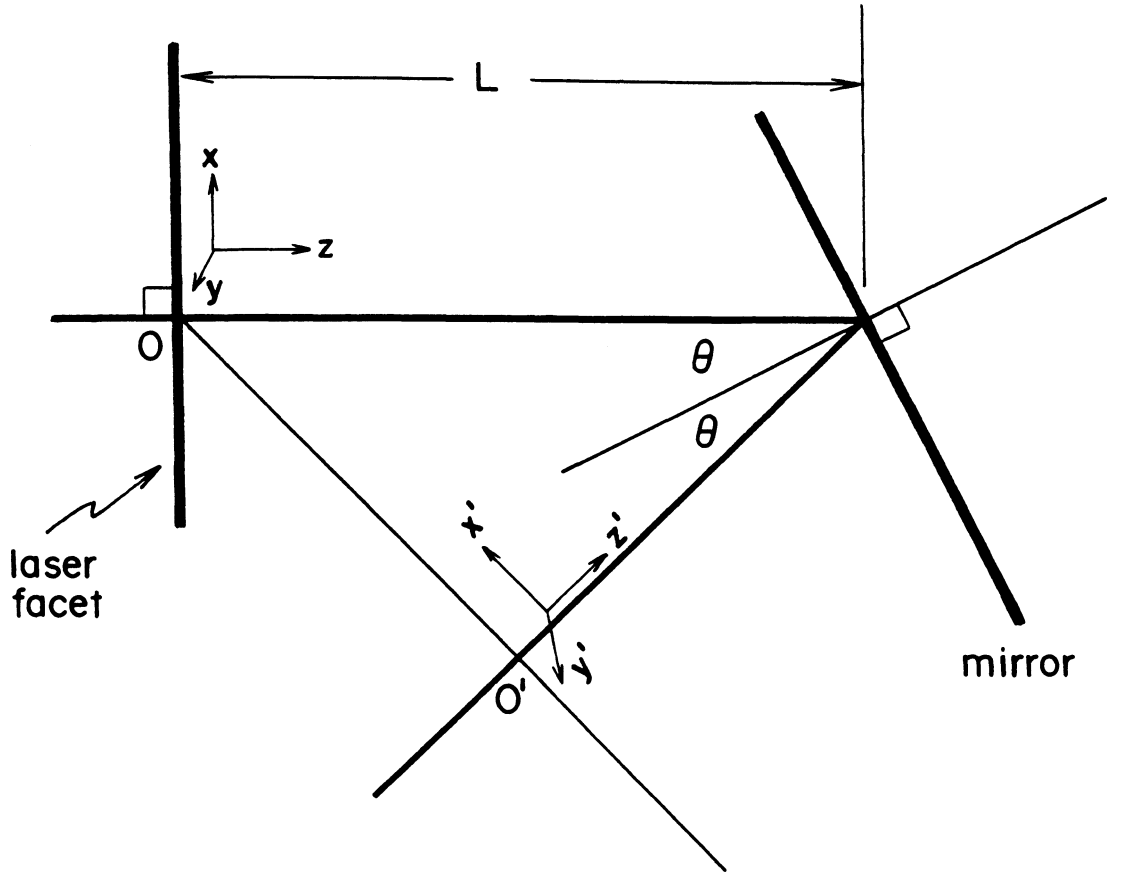

Figure A–1: Geometry of the laser and external mirror used for the theoretical calculation of the optical feedback.

and a similar expression for E_y. $2\omega_{ox}$, $2\omega_x$ are the beam waists of the laser facet and the reflected beam respectively. $k=2\pi/\lambda$ is the wave number, the wavelength is λ, and R_x is the beam radius.

The coupling efficiency, τ , along one dimension is the squared absolute value of the overlap integral of the near field and the reflected far field [31]. For the x dimension

$$\tau_x = \left| \int_{-\infty}^{+\infty} E_x(x,z=0) \cdot E_x'(x',z')dx \right|^2 \qquad (5)$$

Using (1), (2) and (4) in (5), one finds

$$\cos^2 2\theta_x \cdot \tau_x = \left| \int_{-\infty}^{+\infty} E_o \sqrt{\frac{2}{\pi\omega_{ox}\omega_x}} \exp\left[-x^2\left(\frac{1}{\omega_{ox}^2} + \frac{\cos^2 2\theta_x}{\omega_x^2} + \frac{i\pi}{\lambda R_x}\cos^2 2\theta_x\right)\right.\right.$$

$$-2x\left(\frac{L\sin 2\theta_x \cos 2\theta_x}{\omega_x^2} + \frac{i\pi L}{\lambda R_x}\sin 2\theta_x \cos 2\theta_x + \frac{i\pi}{\lambda}\sin 2\theta_x\right.$$

$$\left.\left.\left. -\left(\frac{L^2 \sin^2 2\theta_x}{\omega_x^2} + \frac{i\pi L^2}{\lambda R_x}\sin^2 2\theta_x - i\arctan\left(\frac{\lambda L}{\pi\omega_{ox}^2}\right)\right)\right] dx \right|^2$$

(6)

The change in the path length of the reflected beam over the dimensions of the active region is taken to be negligible. Using the integral solution

$$\int_{-\infty}^{+\infty} \exp\,(-ax^2 - 2bx - c)\,dx = \sqrt{\frac{\pi}{a}}\,\exp\left(\frac{b^2}{a} - c\right) \tag{7}$$

the coupling goes as

$$\sqrt{\frac{\pi}{aa^*}}\,\exp\left[\left(\frac{b^2}{a} - c\right) + \left(\frac{b^2}{a} - c\right)^*\right] \tag{8}$$

In this case

$$a = \frac{1}{\omega_{ox}^2} + \frac{\cos^2 2\theta_x}{\omega_x^2} + \frac{i\pi}{\lambda R_x}\cos^2 2\theta_x \tag{9a}$$

$$b = \frac{L\sin 2\theta_x \cos^2 2\theta_x}{\omega_x^2} + \frac{i\pi}{\lambda}\sin 2\theta_x\left(1 + \frac{L\cos 2\theta_x}{R_x}\right) \tag{9b}$$

$$c = \frac{L^2 \sin^2 2\theta_x}{\omega_x^2} + \frac{i\pi L^2}{\lambda R_x}\sin^2 2\theta_x \tag{9c}$$

For an external cavity length of 160 μm, one can make the approximation $\omega_{ox} << \omega_x$ and after substituting the terms of (9) into equation (8) and keeping only the dominant terms the result is

$$\tau_x = \frac{2\omega_{ox}}{\omega_x} \exp\left[-\frac{k^2}{2} \omega_{ox}^2 \sin^2 2\theta_x \left(1 + \frac{L\cos 2\theta_x}{R_x} \right)^2 \right] \times \exp\left[-\frac{2L^2}{\omega_x^2} \sin^2 2\theta_x \right] \qquad (10)$$

A similar expression is found for τ_y . The total coupling efficiency C, is given by

$$C = \tau_x \tau_y \cos^2 2\theta_x \qquad (11)$$

The effective reflectivity (R_3) of the external mirror can then be determined by multiplying the coupling efficiency by the surface reflectivity of the external mirror. The full expression (8) was numerically calculated and the results were compared to the values obtained using the approximations embodied in Eq.(10). The error increased with angle and was found to be $\leq$ 0.2 % at θ=0 and $\leq$ 3 % at θ=10° for the experimental geometry used (ω_{ox}=1.95 μm, ω_x=75.0 μm, λ=1.3 μm, L=160 μm). Thus the approximate expression provides a good estimate of the coupling efficiency for an offset and rotated Gaussian beam.

REFERENCES

1. G.P. Agrawal and N.K. Dhutta, Long–Wavelength Semiconductor lasers, Van Nostrand Reinhold Company, New York, 1986, Chapter 6.

2. A.P. Bogatov, P.G. Eliseev, L.P. Ivanov, A.S. Logginov, M.A. Manko and K.Ya. Senatorov, "Study of the Single–Mode Injection Laser", IEEE J. Quantum Electron. **QE–9** (2), 392–395, 1973.

3. D. Renner and J.E. Carroll, "Simple System for Broad–band Single–mode Tuning of B.H. GaAlAs Lasers", Electron. Lett. **15** (3), 73–74, 1979.

4. T. Kanada and K. Nawata, "Single–Mode Operation of a Modulated Laser Diode with a Short External Cavity", Opt. Comm. **31** (1), 81–84, 1979.

5. K.R. Preston, K.C. Woolard and K.H. Cameron, "External Cavity Controlled Single Longitudinal Mode Laser Transmitter module", Electron. Lett. **17** (24), 931–933, 1981.

6. H. Kuwahara, H. Imai and M. Sasaki, "Intensity Noise of InGaAsP/InP Lasers Under the Influence of Reflection and Modulation", Opt. Comm. **46** (5,6), 315–322, 1983.

7. K.Y. Liou, "Single–Longitudinal–mode Operation of Injection Laser Coupled to a Grinrod External Cavity", Electron. Lett. **19** (19), 750–751, 1983.

8. J.P. van der Ziel and R.M Mikulyak, "Single–mode Operation of 1.3 μm InGaAsP/InP Buried Crescent Lasers using a Short External Cavity", IEEE J. Quantum Electron. **QE–20** (3), 223–229, 1984.

9. C. Lin, C.A. Burrus, R.A. Linke, I.P. Kaminow, J.S. Ko, A.G. Dentai, R.A. Logan and B.I. Miller, "Short–Coupled–Cavity (SCC) InGaAsP Injection Lasers for CW and High–Speed Single–Longitudinal–Mode Operation", Electron. Lett. **19** (15), 561–562, 1983.

10. W.E. Stephens, T.R. Joseph, T. findakly and B.U. Chen, "Optical Frequency Stabilisation of High Power Laser Diodes under Modulation using Short Optical Waveguides", Electron. Lett. **20** (10), 424–426, 1984.

11. J.R. Andrews, "Enhanced Thermal Stability of Single Longitudinal Mode Coupled Cavity Lasers", Appl. Phys. Lett. **47** (2), 71–73, 1984.

12. G. Wenke, R. Gross, P. Meissner and E. Patzak, "Characteristics of a Compact Three Cavity Configuration", J. of Lightwave Technol. **LT–5** (4), 608–615, 1987.

13. D.T. Cassidy, "Influence on the Steady–State Oscillation Spectrum of a Diode Laser for Feedback of Light Interacting Coherently and Incoherently with the Field Established in the Laser Cavity", Appl. Opt. **23** (13), 2070–2077, 1984.

14. C. Voumard, R. Salathe and H. Weber, "Resonance Amplifier Model Describing Diode Lasers Coupled to Short External Resonators", Appl. Phys. **12**, 369–378, 1977.

15. L.A. Coldren and T.L. Koch, "External Cavity Laser Design", IEEE/OSA J. Lightwave Technol. **LT–2** (6), 1045–1051, 1984.

16. C. Lin, C.A. Burrus and L.A. Coldren, "Characteristics of Single–Longitudinal–Mode Selection in Short–Coupled–Cavity (SCC) Injection Lasers", IEEE/OSA J. Lightwave Technol. **LT–2** (4), 544–549, 1984.

17. G.P. Agrawal, "Generalized Rate Equations and Modulation Characteristics of Extenal Cavity Semiconductor Diode Lasers", J. Appl. Phys. **56** (11), 3110–3115, 1984.

18. J.M. Hammer, "Closed Form Theory of Multicavity Reflectors and the Ouput Power of External Cavity Diode Lasers", IEEE J. Quantum Electron. **QE–20** (11), 1252–1258, 1984.

19. W. Jianglin, Z. Hanyi, W. Qun and Z. Binkun, "Single–Mode Characteristics of Short Coupled–Cavity Semiconductor Lasers", IEEE J. of Quantum Electron. **QE–23** (6), 1005–1009, 1987.

20. K.–Y. Liou, C.A. Burrus and F. Bosch, "Graded–Index–Rod External Coupled–Cavity Laser with Backface Ouput–Monitor–Stabilized Single–Frequency Operation", IEEE/OSA J. of Lightwave Technol. LT–3 (3), 985–987, 1985.

21. K.R. Preston, "Simple Spectral Control Technique for External Cavity Transmitters", Electron. Lett. **18** (25), 1092–1094, 1982.

22. H. Zhang, J. Wang, Q. Wu and B.–K. Zhou, "Mode Hopping Suppression of Short–Coupled–Cavity Semiconductor Lasers" Conference on Lasers and Electro–Optics Technical Digest Series 1987, **6** (OSA, Washington DC 1987) paper MF5.

23. M.R. Matthews, K.H. Cameron, R. Wyatt and W.J. Devlin, "Packaged Frequency–Stable Tunable 20 kHz Linewidth 1.5 μm InGaAsP External Cavity Laser", Electron. Lett. 21 (3), 113–115, 1985.

24. S. Raab, K. Hoffman, M. Gabbert, M.K. Glushkov and Yu.V. Kosichkin, "Application of a Diode Laser with an External Resonator in High Resolution Spectroscopy", Sov. J. Quantum Electron. 11 (8), 1068–1071, 1981.

25. D.T. Cassidy and L.J. Bonnell, "Trace Gas Detection with Short–External–Cavity Diode Laser Transmitter Modules Operating at 1.58 μm", Appl. Opt. **27** (13), 2688–2693, 1988.

26. D.T. Cassidy, "Trace Gas Detection Using 1.3 μm InGaAsP Diode Laser Transmitter Modules", Appl. Opt. **27** (3), 610–614, 1988.

27. E.I. Gordon, "Optical Maser Oscillators and Noise", Bell Syst. Tech. J. , **43**, 507–539, 1964.

28. D.T. Cassidy, "Comparison of Rate–Equation and Fabry–Perot Approaches to Modelling a Diode Laser", Appl. Opt. **22** (21), 3321–3326, 1983.

29. D.T. Cassidy, "Analytic Description of a Homogeneously Broadened Injection Laser", IEEE J. Quantum Electron. **QE–20** (8), 913–918, 1984.

30. E. Hartl and G. Muller, "Transition from Gain Guiding to Index Guiding and Characterisation of 1.55 μm Bridge Contacted Ridge Waveguide Lasers", IEE Proceeedings **134** Pt.J (1), 22–26, 1987.

31. W.B. Joyce and B.C. Deloach, "Alignment of Gaussian Beams", Appl. Opt. **23** (23), 4187–4196, 1984.

32. G.H.B. Thompson, Physics of Semiconductor Laser Devices, John Wiley and Sons, New York 1980, Chapter 2.

33. D.T. Cassidy, "Differential Quantum Efficiency of a Homogeneously Broadened Injection Laser", Appl. Opt. **23** (17), 2870–2873, 1984.

34. C.H. Henry, Chapter 3 in Semiconductors and Semimetals Volume 22, ed. W.T. Tsang, Academic Press, Orlando 1985.

35. J.C. Goodwin and B.K. Garside, "Threshold Variations in Diode Lasers Induced by External Resonator Feedback", IEEE J. of Quantum Electron. **QE–19** (10), 1492–1495, 1983.

36. D. Marcuse, Light Transmission Optics, (Van Nostrand Reinhold, New York, 1972), pg.234.